BUREAU OF RECLAMATION

# Population-Level Consequences of Alternative Delta Export Operations for Sacramento River Winter-Run Chinook Salmon: A Life-Cycle Modeling Framework


California Great Basin Region

Bay-Delta Office


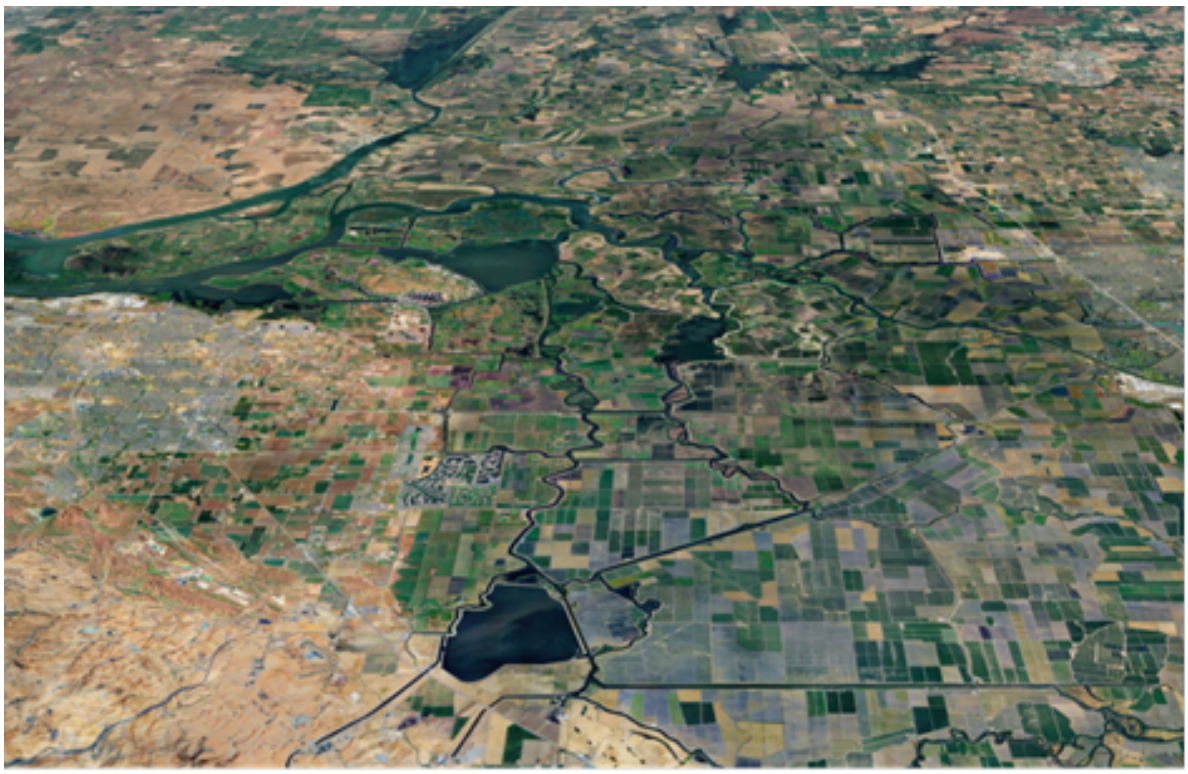

Cover Photo: Aerial photo of the Sacramento-San Joaquin Delta from Google Earth, accessed May 12, 2026.


U.S. Department of the Interior

May 2026

## Mission Statements

The U.S. Department of the Interior protects and manages the Nation's natural resources and cultural heritage; provides scientific and other information about those resources; honors its trust responsibilities or special commitments to American Indians, Alaska Natives, and affiliated Island Communities.

The mission of the Bureau of Reclamation is to manage, develop, and protect water and related resources in an environmentally and economically sound manner in the interest of the American public.

# Population-Level Consequences of Alternative Delta Export Operations for Sacramento River Winter-Run Chinook Salmon: A Life-Cycle Modeling Framework

California Great Basin Region

Bay-Delta Office

*Prepared by*

**Alexander Vaisvil, PhD and Lisa Elliot, PhD**
**Bay-Delta Office**
**Bureau of Reclamation**
**801 "I" Street, Suite 140**
**Sacramento, CA 95814**

**David Ayers, PhD**
**Center for Watershed Sciences**
**University of California, Davis**
**425 La Rue Road**
**Davis, CA 95616**

# Contents



# Tables



# Figures

# Acronyms

| | |
|---|---|
| BY | brood year |
| CDFW | California Department of Fish and Wildlife |
| CPUE | catch-per-unit-effort |
| CV | coefficient of variation |
| CVP | Central Valley Project |
| CVPIA | Central Valley Project Improvement Act |
| CWT | coded wire tag |
| Delta | Sacramento–San Joaquin Delta |
| DJFMP | Delta Juvenile Fish Monitoring Program |
| DSM | Decision Support Model |
| ECO-PTM | Ecological Particle Tracking Model |
| JPE | juvenile production estimate |

| | |
|---|---|
| km | kilometer |
| $km^2$ | square kilometers |
| LCM | life-cycle model |
| LSNFH | Livingston Stone National Fish Hatchery |
| $m^3/s$ | cubic meters per second |
| $M_{age2}$ | first-ocean-year mortality |
| MAPE | mean absolute percent error |
| mm | millimeter |
| NMFS | National Marine Fisheries Service |
| NSE | Nash-Sutcliffe efficiency |
| OAT | one-at-a-time |
| OBAN | Oncorhynchus Bayesian Analysis |
| PFMC | Pacific Fishery Management Council |
| Reclamation | U.S. Department of Interior, Bureau of Reclamation |
| rkm | river kilometer |
| RMSE | root mean square error |
| SacPAS | Salmon Assessment at Chipps and Prediction of Adult Returns |
| SIT | Science Integration Team |
| SRCLCM | Sacramento River Chinook Salmon Life Cycle Model |
| SWFSC | Southwest Fisheries Science Center |
| SWP | State Water Project |
| USFWS | U.S. Fish and Wildlife Service |

# Executive Summary

The U.S. Department of Interior, Bureau of Reclamation (Reclamation) developed a stage-structured lifecycle model for Sacramento River winter-run Chinook Salmon that integrates weekly Ecological Particle Tracking Model (ECO-PTM) through-Delta survival estimates with empirically parameterized ocean demographics to translate Delta survival changes into population-level consequences. We applied three complementary evaluation approaches: (1) a deterministic dose-response across proportional Sacramento–San Joaquin Delta (Delta) survival perturbations (±1%, ±2.5%, ±5%, ±10%) to characterize the translational relationship between Delta survival and equilibrium abundance; (2) a Monte Carlo stochastic decomposition (1,000 iterations) isolating the contribution of each empirically parameterized demographic component to year-50 prediction-interval width; and (3) a paired-iteration comparison using absolute percentage-point perturbations (1%, 2.5%, 5%, 7.5%, 10%) to enable direct comparison with the prior winter-run life-cycle model (Hendrix et al. 2014). Using a synthetic dose-response framework, we found that each 1% proportional change in through-Delta survival shifted deterministic equilibrium abundance by approximately 31 spawners. Under stochastic simulation (1,000 iterations), residual demographic variation from all non-Delta processes produced prediction intervals approximately 16 times wider than the full dose-response range; no synthetic scenario was distinguishable from baseline. The largest perturbation evaluated (+10%) produced an equilibrium of 2,410 spawners. Application to operational alternatives requires scenario-specific ECO-PTM survival estimates; the dose-response framework presented here establishes the translational relationship between Delta survival and population outcomes.

# 1. Introduction

Managing anadromous fish populations in heavily altered estuaries requires linking water infrastructure operations (e.g., releases, diversions, routing) to biological outcomes across the full demographic cycle, from spawning and juvenile rearing through ocean residency and adult return (Hendrix et al. 2014; Moussalli & Hilborn 1986; Zeug et al. 2012). Water operations decisions made at a single constriction, such as water diversion facilities in the southern Sacramento–San Joaquin Delta (Delta), may propagate through the population with lags from three to five years, attenuated or amplified by density dependence, ocean productivity, harvest, and environmental stochasticity (Crozier et al. 2021; Scheuerell et al. 2006). Life-cycle models provide the capability to trace such perturbations forward through all subsequent life stages to assess their ultimate effect on population abundance and viability (Friedman et al. 2019). Here, we use a life-cycle model of Sacramento River winter-run Chinook Salmon (*Oncorhynchus tshawytscha*) to evaluate how changes in through-Delta survival affect long-term population outcomes.

Sacramento River winter-run Chinook Salmon were listed as endangered under the federal Endangered Species Act in 1994 following a population decline from an estimated 117,808 spawners in 1969 to fewer than 200 by the early 1990s (Federal Register 1994; Botsford and Brittnacher 1998). The population spawns exclusively in the mainstem Sacramento River between Keswick Dam (river kilometer (rkm) 486) and Red Bluff Diversion Dam (rkm 391), depending entirely on cold-water releases from Shasta Reservoir for egg survival (National Marine Fisheries Service (NMFS) 2014). The five-year geometric mean escapement for brood years 2021–2025 is 6,481 spawners (California Department of Fish and Wildlife (CDFW) GrandTab 2026). Juvenile outmigrants must transit the Sacramento–San Joaquin Delta, where the Central Valley Project (CVP) and State Water Project (SWP) export pumping generates negative flows in Old and Middle River that entrain migrants into the interior Delta (Grimaldo et al. 2009; Perry et al. 2015, Jensen et al 2025).

Current management tools used to establish loss thresholds quantify juvenile losses only to ocean entry. The juvenile production estimate (JPE) framework tracks the population from spawning through Delta entry and estimates proportional loss attributable to export facilities (NMFS 2019). It does not translate survival changes into population-level consequences. Whether a given reduction in through-Delta survival measurably affects the spawning population three to four years later depends on density dependence, ocean productivity, harvest, and environmental stochasticity across all intervening life stages (Moussalli and Hilborn 1986; Scheuerell et al. 2006; Zeug et al. 2012).

We developed a stage-structured lifecycle model to bridge this gap, translating Ecological Particle Tracking Model (ECO-PTM) Delta survival estimates at weekly temporal resolution into population-level outcomes. The model tracks cohorts through freshwater production, Delta passage, multi-year ocean residency, harvest, and adult return using empirically parameterized demographic rates from published literature and publicly available monitoring data. We applied a synthetic dose-response framework, proportional perturbations to through-Delta survival rather than evaluations of specific operational alternatives, to characterize the translational relationship between Delta survival changes and equilibrium spawner abundance and to evaluate whether that signal is detectable against the background of residual demographic variation. The framework is structured around perturbations to a vital rate (through-Delta survival) rather than perturbations to a specific operational lever (e.g., export reduction), so that the demographic leverage of Delta survival can be evaluated alongside

other life-cycle transition rates (e.g., first-ocean-year mortality, adult en route survival, egg-to-fry survival) that are characterized in the sensitivity analysis (Section 3.4). Translation from a given operational alternative to a change in through-Delta survival is provided by ECO-PTM and is treated here as an external input rather than as a parameter of this model.

# 2. Methods

## Study Area

The study area encompasses the Sacramento River basin from Keswick Dam (rkm 486) through the Delta to the Pacific Ocean at the Golden Gate Bridge (rkm 0) (Figure 1). Winter-run Chinook salmon spawn in a 95-kilometer (km) reach of the mainstem Sacramento River below Keswick Dam, the only remaining spawning habitat following the construction of Shasta Dam in 1945. Juveniles rear in the Sacramento River and migrate downstream through the Delta, an approximately 2,900 square kilometers ($km^2$) tidally influenced estuary where the CVP and SWP pumping plants can export over 400 cubic meters per second ($m^3/s$) during peak operations, generating hydrodynamic gradients that entrain outmigrating juvenile salmonids into the interior Delta (Grimaldo et al. 2009; Perry et al. 2015). After exiting the Delta, juveniles enter San Francisco Bay and finally the Pacific Ocean, where they reside for one to three years before returning to spawn (Quinn 2018).

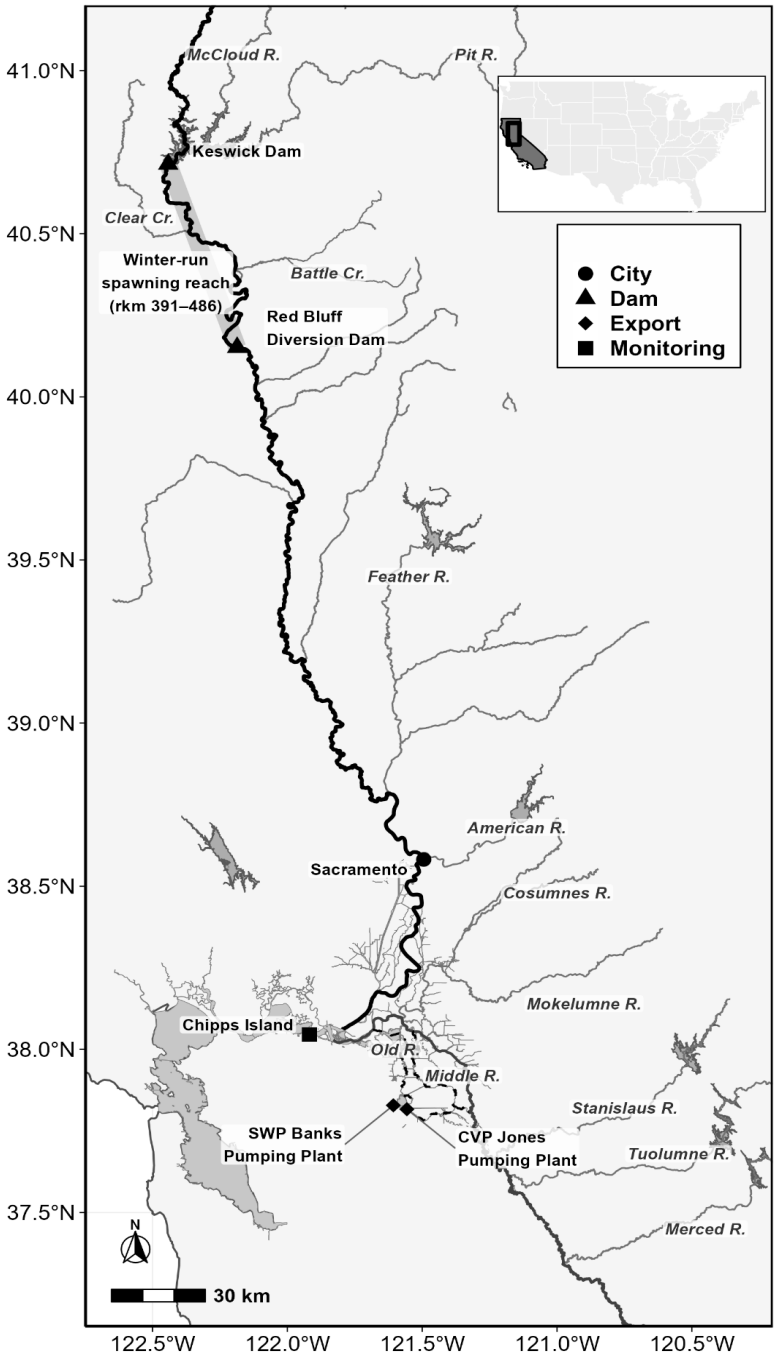


Note: The Sacramento River mainstem (heavy black line) is shown with major Central Valley tributaries (grey lines). Old and Middle Rivers (dashed) are the primary export-influenced channels in the south Delta. Diamond symbols mark the Central Valley Project Pumping Plant and the State Water Project Pumping Plant. The shaded reach between Keswick Dam and Red Bluff Diversion Dam indicates the winter-run Chinook salmon spawning habitat.

**Figure 1. Study Area Encompassing the Sacramento River Basin and Sacramento–San Joaquin Delta, California**

## Model Framework

Reclamation developed a stage-structured, temporally explicit life-cycle model (LCM) for Sacramento River winter-run Chinook Salmon designed to evaluate the population-level consequences of changes in through-Delta survival. The model tracks annual cohorts from adult spawning through freshwater rearing, Delta outmigration, multi-year ocean residency, fishery harvest, and river return (Figure 2). The model resolves weekly variation in Delta passage survival but does not resolve spatial routing within the Delta; combined through-Delta survival from ECO-PTM is used as a single weekly input. The architecture supports three mutually exclusive execution modes: (1) calibration, in which observed escapement is supplied as spawner input each year and first-ocean-year mortality ($M_{age2}$) is optimized to minimize prediction error; (2) validation, which applies literature-derived parameters without fitting to quantify the gap between published demographic estimates and observed population dynamics; and (3) forward simulation, in which the population is projected over a 50-year horizon using calibrated parameters and Monte Carlo stochastic draws.

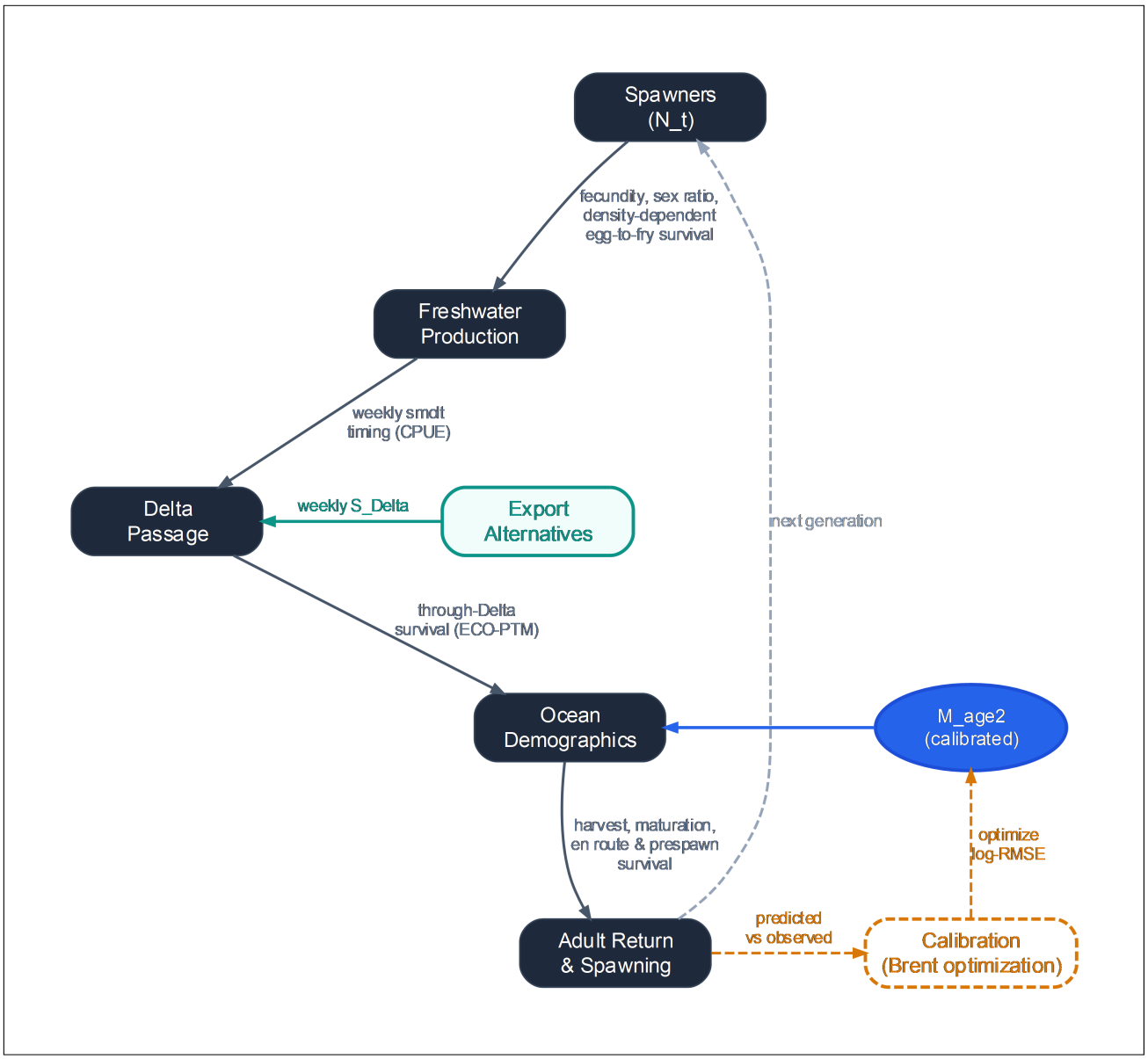


Notes: Dark boxes represent demographic stages; the blue ellipse indicates the calibrated first-ocean-year mortality parameter ($M_{age2}$); the teal box represents the management decision point where export alternatives enter the model through scenario-specific Delta survival values; and dashed amber arrows indicate the calibration feedback loop in which predicted spawner returns are compared to observed escapement to optimize $M_{age2}$ via log-RMSE minimization.

**Figure 2. Simplified Conceptual Diagram of the Winter-run Chinook Salmon Life Cycle Model**

# Freshwater Production

We modeled annual freshwater production as a sequential chain of density-dependent and density-independent survival stages, converting spawner abundance into the number of natural-origin smolts arriving at the Delta. The freshwater production chain for brood year *t* is:

$$N_{eggs,t} = N_t \times p_{f,t} \times F_t$$

$$N_{fry,t} = N_{eggs,t} \times S_{e2f,t}$$

$$N_{smolt,t}^{nat} = N_{fry,t} \times S_{rear,t} \times S_{outmig,t}$$

where $N_t$ is spawner escapement in brood year $t$, $p_{f,t}$ is the proportion female, $F_t$ is fecundity (eggs per female), $S_{e2f,t}$ is egg-to-fry survival (density-dependent), $S_{rear,t}$ is fry-to-smolt rearing survival, $S_{outmig,t}$ is smolt outmigration survival from the river to the Delta, and $N_{smolt,t}^{nat}$ is the number of natural-origin Delta entrants. Year-specific upstream vital rates were obtained from the Salmon Assessment at Chipps and Prediction of Adult Returns (SacPAS) JPE data for brood years 2009–2025 (Table 1).

**Table 1. Upstream Vital-Rate Parameters from the SacPAS JPE Database**

| Parameter | Symbol | Period mean (BY 2009–2025) | Range | Note |
|---|---|---|---|---|
| Fecundity | F | 5,066 eggs/female | 3,353–6,037 | Range across all available BY |
| Sex ratio (proportion female) | p_f | 0.554 | 0.383–0.783 | CV = 0.147 |
| Egg-to-fry survival | U | 0.188 | — | Period mean shown for reference; replaced in the model by the Beverton–Holt prediction (Eq. 1) in simulation, and by year-specific values in calibration. |
| Rearing survival | S_rear | 0.520 | varies by BY | Smolt survival from fry to outmigration |
| Outmigration survival | S_outmig | 0.423 | varies by BY | Survival to Delta entry |
| Prespawn survival | S_prespawn | 0.983 | varies by BY | CV ≈ 0.01; treated as effectively constant |

Notes:
Period means are computed across BY 2009–2025; ranges reflect the full available time series (n = 33 brood years).
In calibration mode, year-specific values from historical_data_ts override these means. In simulation mode, period means are used (with stochastic draws for sex ratio).
Key: BY = brood year; CV = coefficient of variation

Density-dependent egg-to-fry survival followed the Beverton–Holt formulation of Martin et al. (2017; Figure 3):

$$S_{e2f} = U_0 / (1 + N_r / D)$$

where $U_0 = 0.399$ is the density-independent maximum survival, $N_r$ is the number of redds (estimated as $N_r = N_t \times p_f$, assuming one redd per female), and $D = 1{,}028$ is the carrying capacity in redds. The functional form follows Martin et al. (2017). The parameter values $U_0 = 0.399$ and D = 1,028 redds adopted here are calibrated defaults of the SacPAS Fish Model v3.1, which reframed the Martin et al. (2017) functional form in units of spawned female carcasses (redds) using additional years of egg-to-fry data. Martin et al.'s (2017) original fitted carrying capacity (K = 9,107) was expressed in units of total population escapement and is therefore not directly comparable. A

further recalibration incorporating temperature-dependent fry mortality and additional brood years is in progress (Beer 2024) and will become the SacPAS Fish Model default when finalized. Environmental variation around the Beverton–Holt prediction was modeled as a multiplicative lognormal perturbation with a coefficient of variation (CV) of 0.65, derived from the ratio of observed to predicted egg-to-fry survival across 17 brood years (BY 2009–2025).

Hatchery contributions from the Livingston Stone National Fish Hatchery (LSNFH) were added at the Delta entry stage. Total Delta entrants were $N_{Delta,t} = N_{smolt,t}^{nat} + N_{hat,t}$, where $N_{hat,t}$ is hatchery-origin juvenile production entering the Delta. In calibration mode, the observed sex ratio from SacPAS was used directly for egg production. In forward simulation mode, the proportion of female spawners emerged from the sex-specific ocean maturation model (Section 2.5) rather than being set to a constant value, so that egg production responds naturally to changes in hatchery composition and age structure.

Hatchery juvenile production $N_{hat,t}$ was obtained directly from the SacPAS hatchery JPE record for each brood year in calibration mode. In forward simulation mode, $N_{hat,t}$ was drawn from a lognormal distribution parameterized by the long-term mean and CV (0.41) of annual hatchery JPE values from SacPAS, or set to the long-term mean for deterministic runs. Total weekly Delta entrants in week w were obtained by applying the empirical Delta Juvenile Fish Monitoring Program (DJFMP) - derived weekly timing distribution (Section 2.4) to the combined natural-plus-hatchery total: $N_{Delta,w} = (N_{smolt,t}^{nat} + N_{hat,t}) \times p_w$, where $p_w$ is the empirical proportion of total annual passage assigned to week w. This formulation treats natural-origin and hatchery-origin smolts as sharing a single timing distribution. In practice, LSNFH winter-run releases occur primarily in late January through February (typical release size ~90–110-millimeter (mm) fork length), whereas the DJFMP-derived distribution reflects mostly natural-origin passage and shows peak passage in mid-December (water year week 11). Applying the combined-stock timing distribution to the hatchery component therefore advances some hatchery-origin Delta entrants to earlier weeks than reflect actual release timing, which may correspond to outmigration conditions less representative of the hatchery cohort. Reconciliation of the timing module with cohort-resolved hatchery release records is a planned refinement.

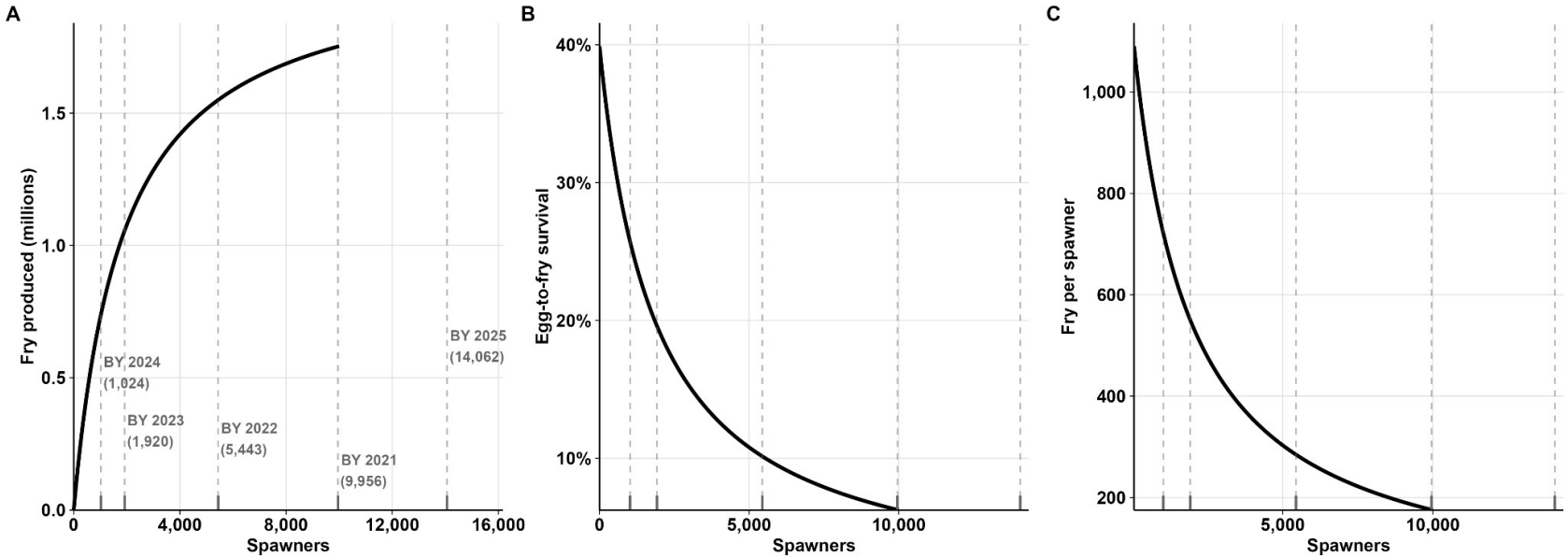


Source: CDFW GrandTab 2025

Notes: Dashed vertical lines and rug marks indicate observed escapement for the five most recent brood years (BY 2021–2025). Graph A shows the Total Fry Produced as a Function of Spawner Abundance; Graph B is Egg-to-Fry Survival Rate, Declining with Increasing Spawner Density; and Graph C is the Fry Produced per Spawner, Illustrating the Compensatory Dynamic Where per-capita Production is Highest at Low Abundance.

**Figure 3. Beverton–Holt Density-dependent Freshwater Production for Sacramento River Winter-run Chinook Salmon**

## Delta Passage

Reclamation distributed total annual Delta entrants across weeks of the water year using empirical catch-per-unit-effort (CPUE)-based timing distributions derived from the DJFMP trawl data (1976–2025; U.S. Fish and Wildlife Service (USFWS) 2026, Figure 4). Peak passage occurred at water year week 11 (approximately mid-December), defined as the week with the highest mean proportion of annual passage across the 1976–2025 record. The number of smolts entering the ocean in week w was:

$$N_{\text{ocean,w}} = N_{\text{Delta,w}} \times S_{\Delta,\text{w}}$$

where $N_{\text{Delta,w}}$ is the number of Delta entrants in week $w$ and $S_{\Delta,\text{w}}$ is the combined through-Delta survival for that week, obtained from ECO-PTM (Perry et al. 2015, 2018). Total annual ocean entry was the sum across all migration weeks:

$$N_{\text{ocean}} = \Sigma N_{\text{ocean,w}}.$$

For the synthetic dose-response evaluation, proportional perturbations were applied to weekly survival: $S_{\Delta,\text{w}}^{*} = S_{\Delta,\text{w}} \times (1 - \delta)$, where $\delta > 0$ represents degraded Delta conditions and $\delta < 0$ represents improved conditions relative to baseline. These perturbations are synthetic manipulations of through-Delta survival, not representations of specific CVP or SWP operational alternatives.

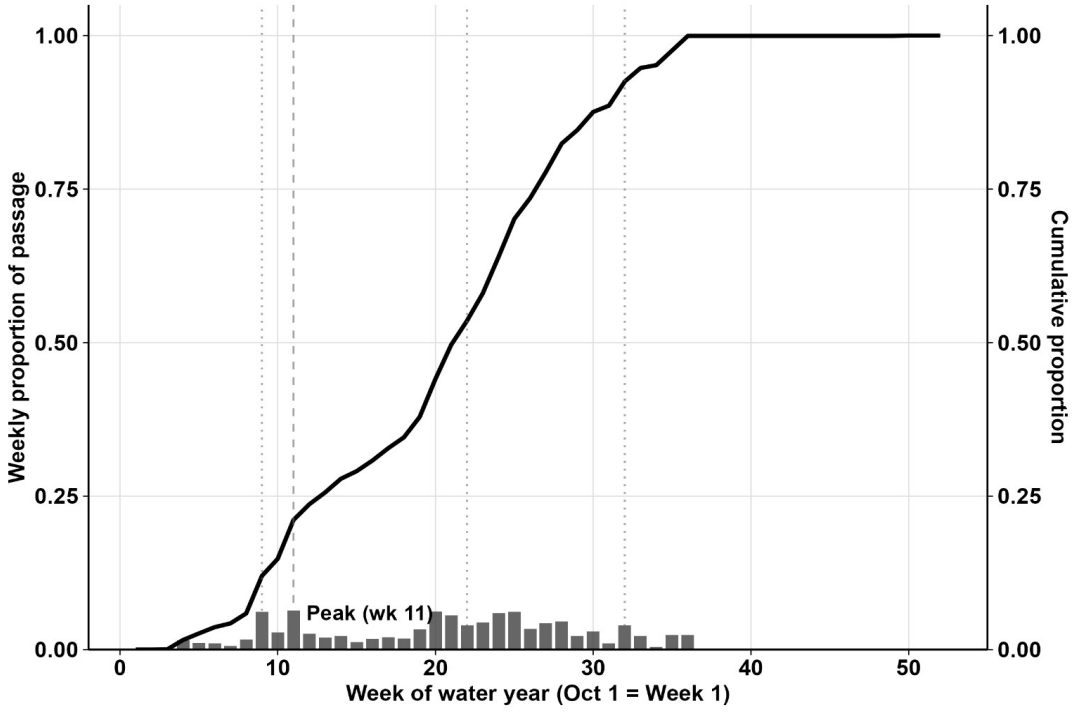


Notes: Bars show the proportion of total annual passage occurring in each week of the water year (October 1 = Week 1). The solid line shows the cumulative proportion of passage. The dashed vertical line marks the peak migration week (week 11, approximately mid-December), defined as the week with the highest mean proportion of annual passage across the 1976–2025 record. Dotted vertical lines indicate the 10th percentile (week 9), median (week 22), and 90th percentile (week 32) of the cumulative distribution.

**Figure 4. Historical Average Weekly Delta Entry Timing Distribution for Winter-run Chinook Salmon Juveniles**

## Ocean Demographics (Sex-Weighted, Origin-Specific)

The ocean phase tracked four population segments, natural-origin males, natural-origin females, hatchery-origin males, and hatchery-origin females, through age classes two through four (Figure 5). All mortality and harvest rates were applied identically across segments; only maturation probabilities differed by origin and sex. Base natural mortality rates were adopted from Winship et al. (2014): first-ocean-year mortality $M_{age2} = 0.50$ (literature value; calibrated to approximately 0.971) and adult annual natural mortality $M_{adult} = 0.20$. The initial sex ratio at ocean entry was assumed to be 50:50.

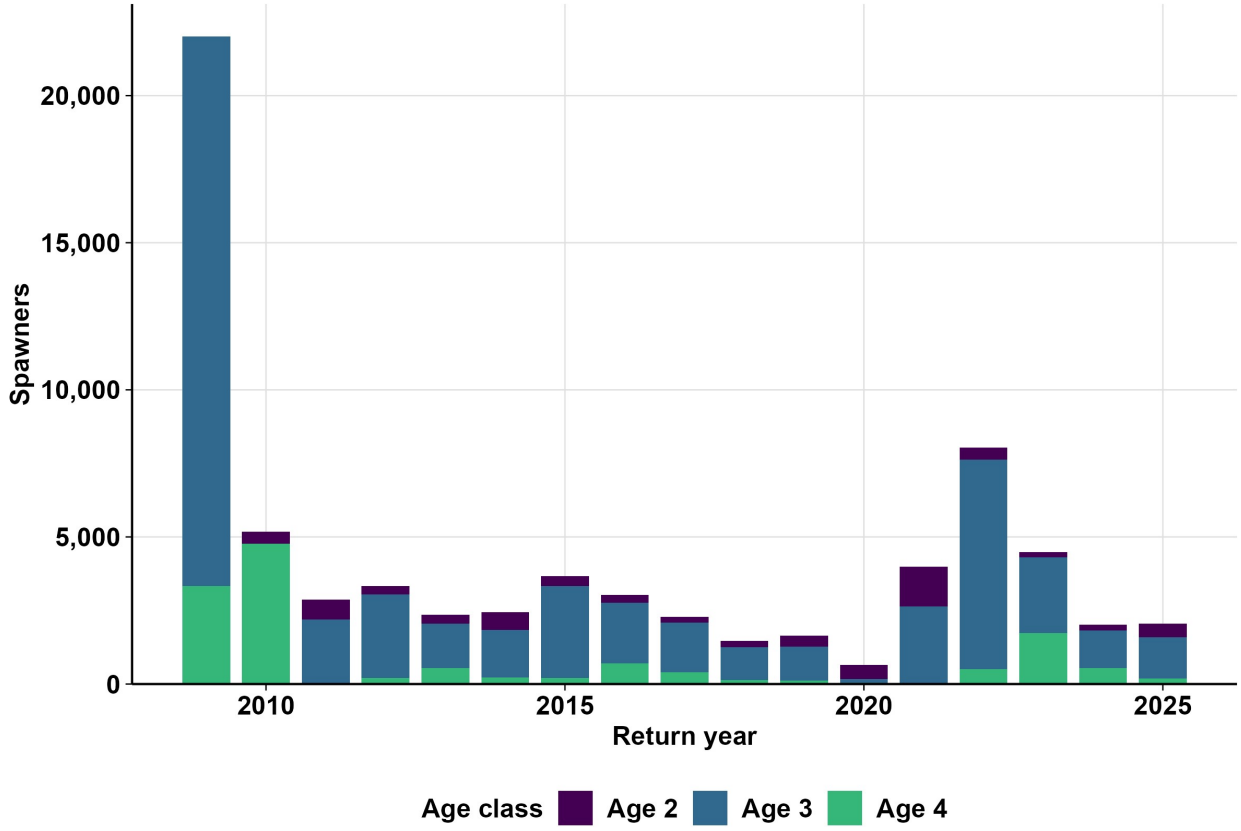


Notes: Stacked bars show contributions from age-2 (jacks), age-3, and age-4 fish. Return years 2009–2012 reflect cohorts originating from warmup brood years (2005–2008), which were initialized from historical escapement rather than modeled from prior generations. The large age-3 bar in 2009 reflects the high brood-year 2006 escapement propagated through the model.

**Figure 5. Model-predicted Age Composition of Spawner Returns by Return Year during the Calibration Period (return years 2009–2025, n = 17)**

Sex-specific maturation probabilities were derived from a coded-wire tag (CWT)-based cohort reconstruction (Chen et al. 2023; Table 2). Because female maturation at ages two and three is substantially higher than male maturation, particularly for natural-origin fish, where female $m_3 = 0.95$ versus male $m_3 = 0.53$, nearly all females return by age 3, leaving the age-4 pool approximately 87–90% male. The model computed female spawners at each age and used them directly for egg production in the forward simulation feedback loop:

$$N_{eggs,t+1} = N_{female,y} \times F$$

where $N_{female,y}$ is the total number of female spawners returning in year $y$ (summed across all ages and origins) and $F$ is fecundity (eggs per female). This formulation allows the emergent sex composition of returns, which varies with hatchery fraction and age structure, to influence reproductive output, rather than assuming a constant female fraction.

**Table 2. Brood-year-Specific Ocean Harvest Impact Rates ($h_3$, $h_4$) Used in the Model**

| Brood Year | Harvest Rate for Age 3 Fish | Harvest Rate for Age 4 Fish | Source / Note |
|---|---|---|---|
| 2000 | 0.218 | 0.195 | O'Farrell & Satterthwaite (2015) |
| 2001 | 0.000 | 0.390 | Chen et al. (2023) CWT cohort reconstruction |
| 2002 | 0.255 | 0.250 | Chen |
| 2003 | 0.174 | 0.192 | Chen |
| 2004 | 0.177 | 0.176 | Chen |
| 2005 | 0.172 | 0.000 | Chen; $h_4 \rightarrow 0$ (RY 2009 closure) |
| 2006 | 0.000 | 0.000 | Chen; $h_3 \rightarrow 0$ (RY 2009 closure) |
| 2007 | 0.000 | 0.205 | Chen |
| 2008 | 0.148 | 0.551 | Chen |
| 2009 | 0.321 | 0.197 | Chen |
| 2010 | 0.128 | 0.284 | Chen |
| 2011 | 0.186 | 0.284 | Chen |
| 2012 | 0.166 | 0.025 | Chen |
| 2013 | 0.016 | 0.215 | Chen |
| 2014 | 0.112 | 0.380 | Chen |
| 2015 | 0.188 | 0.249 | Chen |
| 2016 | 0.140 | 0.958 | Chen |
| 2017 | 0.937 | 0.000 | Chen |
| 2018 | 0.147 | 0.152 | PFMC (open seasons) |
| 2019 | 0.152 | 0.000 | Pacific Fishery Management Council; $h_4 \rightarrow 0$ (RY 2023 closure) |
| 2020 | 0.000 | 0.000 | Pacific Fishery Management Council; $h_3$, $h_4 \rightarrow 0$ (RY 2023, 2024 closures) |
| 2021 | 0.000 | 0.016 | Pacific Fishery Management Council; $h_3 \rightarrow 0$ (RY 2024 closure) |
| 2022 | 0.016 | — | Pacific Fishery Management Council; $h_4$ not yet observed |

Sources: O'Farrell & Satterthwaite (2015) for BY 2000; Chen et al. (2023) for BY 2001–2017; PFMC Preseason Report III for BY 2018–2022.

Note:

$h_3$ = age-3 ocean fishery impact rate; $h_4$ = age-4 ocean fishery impact rate.

The model zeros h to 0.000 when the raw value > 0.50 AND the corresponding return year (BY+age) falls in the legacy full-PFMC closure set {2008, 2009}; recent winter-run closures (RY 2023–2024) are handled via PFMC overrides.

'—' = not yet observed.

Brood-year-specific ocean harvest impact rates ($h_3$, $h_4$) were assembled from Chen et al. (2023) for BY 2001–2017, O'Farrell and Satterthwaite (2015) for BY 2000, and Pacific Fishery Management Council (PFMC) Preseason Report III for BY 2018–2022 (PFMC 2022). Full PFMC fishery closures

(2008, 2009) were automatically zeroed; recent closures (return years 2023–2024, for winter-run protection) were handled through direct harvest rate overrides for affected brood years (Table 3). For forward projections, harvest was drawn from a Beta distribution parameterized from the observed mean and standard deviation of age-3 rates. Adult en route survival, the probability that returning adults survive upstream migration from the ocean to the spawning tributary ($S_{enroute}$ = 0.80), and prespawn survival, the probability of surviving from arrival at the spawning grounds through spawning ($S_{prespawn}$ = 0.98) were derived from the Central Valley Project Improvement Act (CVPIA) Science Integration Team (SIT) Winter-run Chinook salmon Decision Support Model (DSM).

**Table 3. Sex-Specific, Origin-Specific Maturation Probabilities Used in the Ocean Demographic Model**

| Age | Origin | Male | Female | Combined-sex |
|---|---|---|---|---|
| 2 | Natural | 0.12 | 0.07 | 0.10 |
| 2 | Hatchery | 0.21 | 0.02 | 0.08 |
| 3 | Natural | 0.53 | 0.95 | 0.75 |
| 3 | Hatchery | 0.89 | 0.97 | 0.93 |
| 4 | Both | 1.00 | 1.00 | 1.00 |

Source: Chen et al. 2023

Note: Combined-sex values are trimmed brood-year means.

# Calibration

Reclamation designated $M_{age2}$ as an absorptive calibration parameter to account for all unmodeled mortality across the life cycle, including ocean density dependence, predation, disease, environmental stochasticity, and measurement error in upstream production estimates. We optimized $M_{age2}$ using Brent's bounded univariate search algorithm over the interval [0.10, 0.995] to minimize the log-scale root mean square error (log-RMSE) between model-predicted and observed spawner returns for brood years 2005–2025 (with brood years 2005–2008 serving as a spin-up period to populate all age classes). The fitting objective compared model-predicted and observed spawner returns for return years 2009–2025. During calibration, observed escapement was supplied as the spawner input for each brood year rather than using the model's own predicted returns, preventing prediction errors from compounding across brood years. Predictive performance was assessed through 5-fold cross-validation (Figure 6), in which the 17 calibration brood years (BY 2009–2025) were randomly partitioned into five approximately equal folds (seed = 42). $M_{age2}$ was re-estimated on each training fold using the same Brent optimization, and prediction error was evaluated on the held-out fold. Return years lacking complete age-class coverage were excluded from the fitting objective within each fold, consistent with the full-data calibration. Summary metrics included RMSE, mean absolute percent error (MAPE), and Nash-Sutcliffe efficiency (NSE).

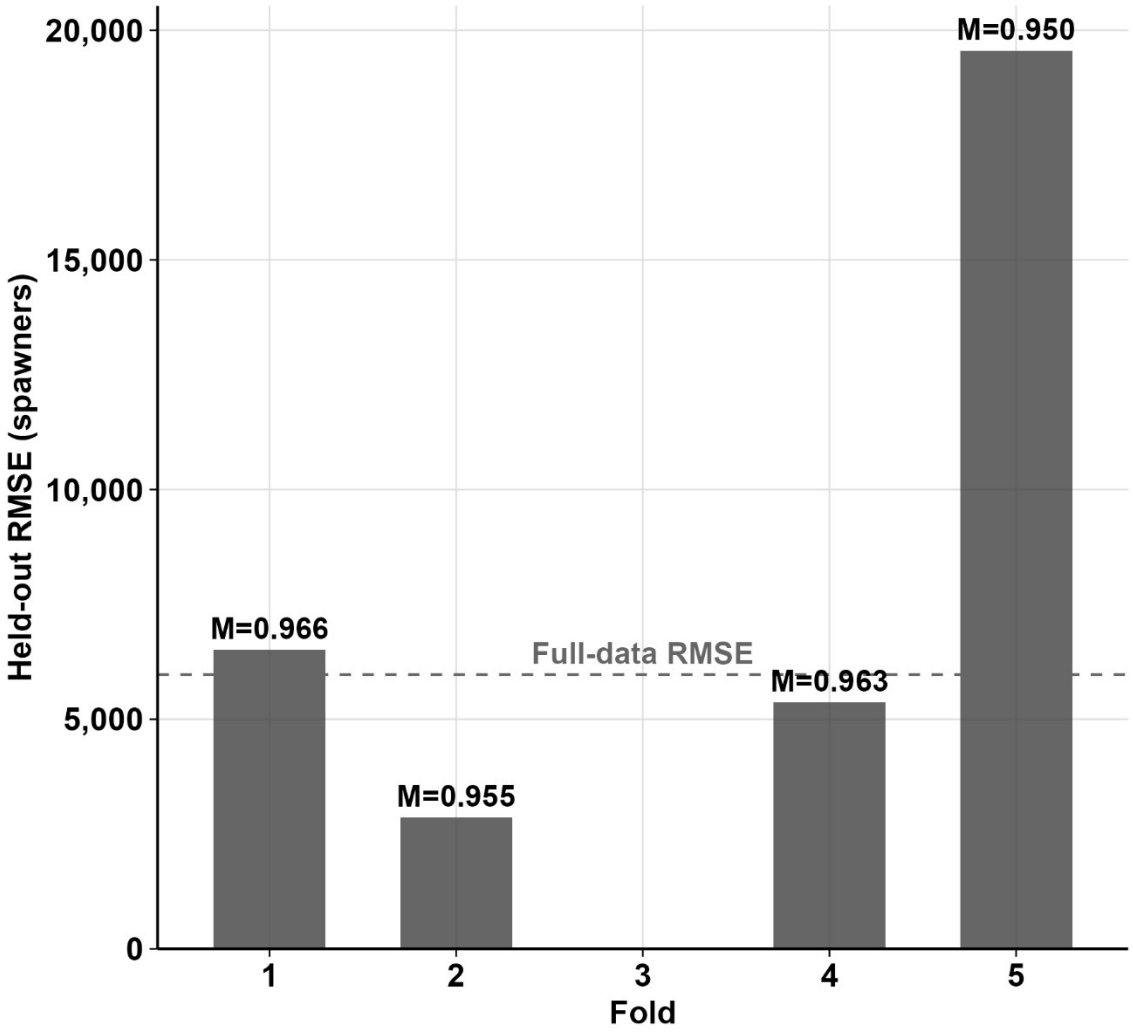


Notes: Each bar shows the held-out root mean square error (RMSE) for one-fold, with the fold-specific re-estimated Mage2 value labeled above the bar. The dashed horizontal line indicates the full-data RMSE (4,081 spawners)

**Figure 6. Five-fold Cross-Validation of the Calibrated $M_{age2}$ Parameter**

# Stochasticity and Scenario Evaluation

Forward projections used a Monte Carlo framework (1,000 iterations per scenario) with seven empirically parameterized stochastic components (Table 4), each parameterized from observed variation in the calibration period or from Chen et al. (2023). Lognormal draws used bias correction ($\mu_{log} = \log(\mu) - \frac{1}{2}\sigma^2_{log}$) to ensure the expected value equaled the deterministic central estimate.

**Table 4. Stochastic Components Activated for Forward Simulation**

| Component | Distribution | CV | Source |
|---|---|---|---|
| $M_{age2}$ (first-ocean-year mortality) | Lognormal | 0.08 | Calibration residuals (n = 17 BY) |
| Egg-to-fry survival | Lognormal | 0.65 | SacPAS observed / Beverton–Holt predicted ratios |
| Ocean harvest rate | Beta (α, β) | dynamic | Chen et al. (2023) + PFMC age-3 rates |
| Hatchery juvenile production | Lognormal | 0.41 | SacPAS release totals (n = 16 years) |
| Sex ratio | Lognormal | ~0.15 | SacPAS observed sex ratios |
| Maturation, natural-origin age 3 | Lognormal | 0.19 | Chen et al. (2023) trimmed BY means |
| Maturation, hatchery-origin age 3 | Lognormal | 0.08 | Chen et al. (2023) trimmed BY means |

Key:
BY = Brood Year
PFMC = Pacific Fishery Management Council
SacPAS = Salmon Assessment at Chipps and Prediction of Adult Returns

Three stochastic treatments were applied to each scenario to decompose uncertainty (Figure 7): (1) deterministic (point estimates for all parameters), (2) $M_{age2}$-only (isolating the absorptive first-ocean-year parameter), and (3) full stochastic (all seven components active). Population viability was assessed using quasi-extinction frequency (proportion of iterations with spawner abundance below 250; Lindley et al. 2007) and the proportion of iterations falling below a minimum viable population threshold of 2,500 spawners (Lindley et al. 2007).

The dose-response framework applied bidirectional proportional perturbations to through-Delta survival at ±1%, ±2.5%, ±5%, and ±10%, producing 9 scenarios (1 baseline + 8 perturbations) × 3 stochastic treatments = 27 Monte Carlo configurations. The ±10% upper bound was selected to match the perturbation range used in the Sacramento River Chinook Salmon Life Cycle Model (SRCLCM) analysis (Hendrix et al. 2014), enabling direct paired-iteration comparison between the two frameworks (Section 3.3). The deterministic dose-response is approximately linear across this range, so wider perturbations would primarily extrapolate the same slope rather than reveal additional structural behavior. Each perturbation scales weekly ECO-PTM survival proportionally (e.g., a −10% perturbation reduces a baseline weekly survival of 0.42 to 0.378). These are synthetic manipulations designed to characterize the translational relationship between Delta survival changes and population outcomes, not evaluations of specific operational alternatives.

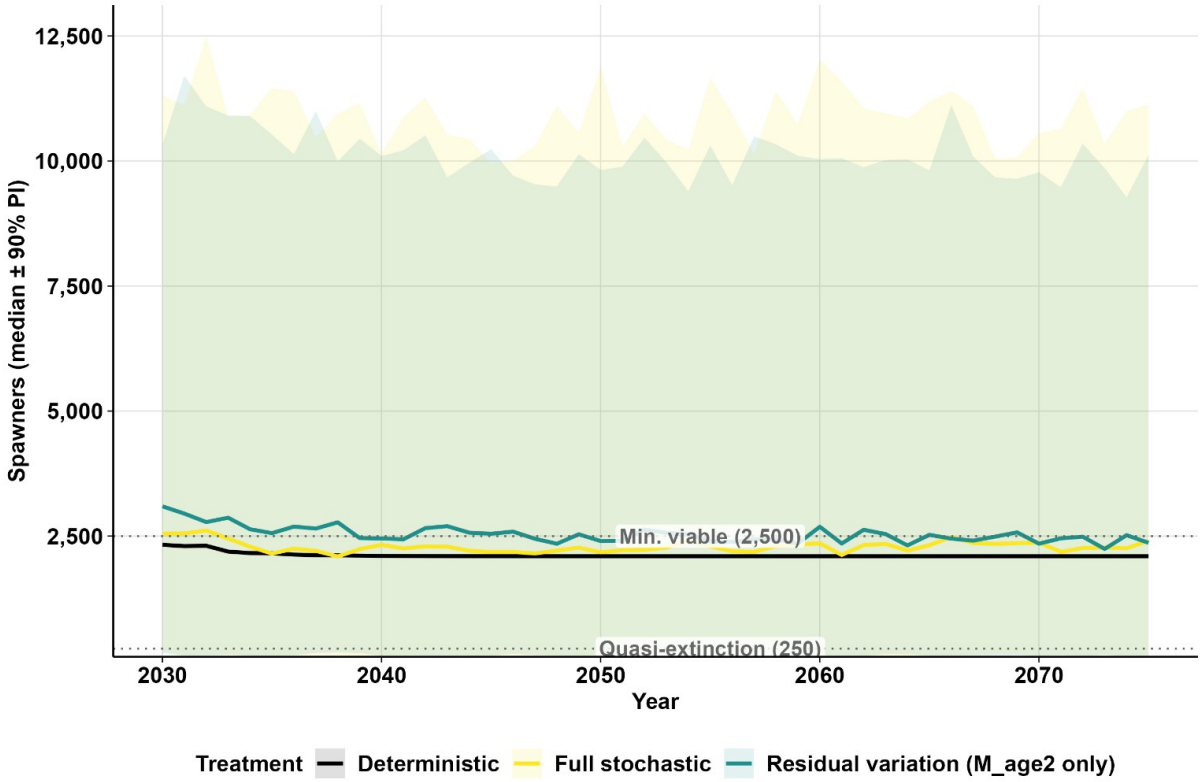


Notes: The deterministic treatment (black) uses point estimates for all parameters. The $M_{age2}$-only treatment (green) adds stochastic variation in the calibrated absorptive first-ocean-year parameter (lognormal, CV = 0.08), which captures all unmodeled demographic processes. The full stochastic treatment (blue) activates all seven empirically parameterized components: $M_{age2}$, egg-to-fry survival, ocean harvest rate, hatchery juvenile production, sex ratio, natural-origin age-3 maturation, and hatchery-origin age-3 maturation (see Table 4). Solid lines show median trajectories; shaded ribbons show 5th–95th percentile envelopes. Dotted horizontal lines indicate the quasi-extinction threshold (250 spawners; Lindley et al. 2007) and minimum viable population size (2,500 spawners; Lindley et al. 2007).

**Figure 7. Baseline Population Trajectories under Three Stochastic Treatments over a 50-year Projection Horizon (1,000 Monte Carlo iterations per treatment)**

# Sensitivity Analysis

Reclamation evaluated parameter sensitivity using a one-at-a-time (OAT) approach (Morris 1991), perturbing each of 15 demographic parameters ±20% from baseline while holding all others constant. The response metric was deterministic equilibrium spawner abundance from a 50-year forward simulation (mean of last 10 years), which captures the density-dependent feedback loop that the calibration-mode metric cannot. Parameters included nine scalar constants ($M_{age2}$, $M_{adult}$, three maturation rates, adult en route survival, prespawn survival, and two Beverton–Holt density-dependence parameters: maximum egg-to-fry survival $U_0$ and carrying capacity D) and six year-specific vectors (fecundity, rearing survival, outmigration survival, hatchery juvenile production, harvest rates, and through-Delta survival), all perturbed ±20% from baseline. $M_{age2}$ was perturbed on the survival scale (±20% of $1 - M_{age2}$) rather than the mortality scale to maintain proportional comparability. Parameters near feasible boundaries were capped at biologically plausible limits (e.g., bounding survival between zero and one).

## Paired Scenario Comparison

To evaluate whether Delta survival changes produce a systematic effect on population outcomes when demographic noise is controlled, Reclamation implemented a paired-iteration Monte Carlo comparison. For each of 1,000 iterations, we set the random number generator seed to the iteration index, ran the baseline scenario, reset the seed to the same value, and ran the alternative scenario. This ensured that both runs experienced identical stochastic draws for $M_{age2}$, egg-to-fry survival, harvest, hatchery production, and all other stochastic components; the only difference between paired runs was the Delta survival perturbation. We evaluated absolute perturbations (1, 2.5, 5, 7.5, and 10 percentage-point reductions in through-Delta survival) to enable direct comparison with the SRCLCM analysis. The absolute perturbation approach subtracts a fixed value from the weekly Delta survival estimate rather than scaling it proportionally. Metrics included mean 10-year abundance with 95% central interval, the percent difference in mean abundance relative to baseline, and the probability that the 3-year rolling sum of natural-origin abundance fell below 2,500 spawners.

# 3. Results

## Calibration

The Brent optimization converged to a calibrated $M_{age2}$ = 0.971 (97.1% first-ocean-year mortality; 2.9% survival), a departure of +47.1 percentage points from the Winship et al. (2014) literature value of 0.50. Using the literature estimate ($M_{age2}$ = 0.50), the model produced an RMSE of 106,778 spawners, approximately 18 times the calibrated value, reflecting the degree to which the absorptive parameter must depart from published all-stock means to match observed winter-run dynamics. Calibration reduced RMSE to 5,969 spawners (88% reduction) with a mean bias of −50 spawners (Figure 8). Year-to-year predictive skill remained limited: the NSE was −1.82 and the MAPE was 112.8%.

Cross-validation confirmed that the calibrated parameter was robust to data subsetting (Figure 6). All five folds converged. Re-estimated M_age2 ranged from 0.944 to 0.966 (mean = 0.959, SD = 0.009), with held-out RMSE ranging from 1,825 to 11,881 spawners (mean = 5,137) and held-out MAPE from 52.3% to 98.6% (mean = 78.6%).

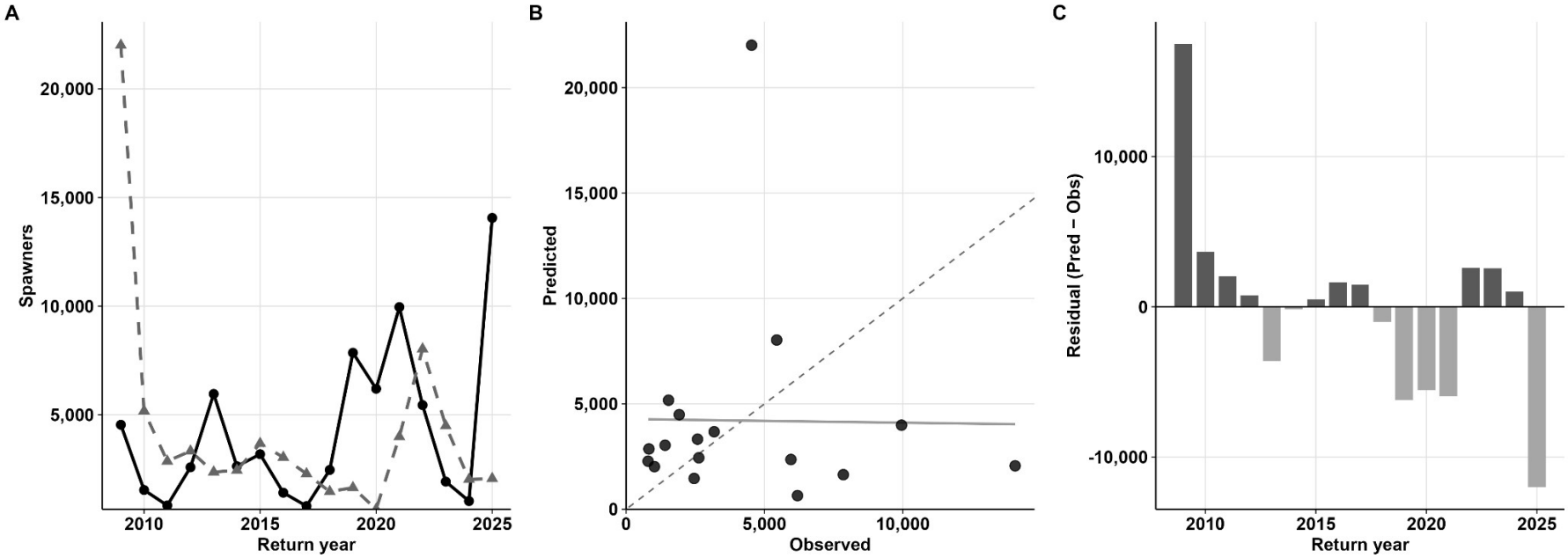


Notes: Graph A shows Time series of observed (black circles, solid line) and predicted (grey triangles, dashed line) spawner abundance; Graph B shows Predicted versus observed scatter; the dashed line indicates perfect 1:1 agreement and the grey line shows the ordinary least-squares fit; and Graph C shows Residuals (predicted minus observed) by return year; positive values indicate overprediction and negative values indicate underprediction.

**Figure 8. Calibration Diagnostics for the Life Cycle Model Fitted to Observed Escapement for Brood Years 2009–2025 by Optimizing a Single Parameter ($M_{age2}$) to Minimize Log-root Mean Square Error**

## Dose-Response

Proportional perturbations to through-Delta survival produced a symmetric, monotonic dose-response relationship with equilibrium spawner abundance (Figure 9). Each 1% change in Delta survival translated to approximately 31 additional or fewer spawners at deterministic equilibrium, a linear relationship across the ±10% perturbation range as expected from the multiplicative model structure. A 10% improvement in through-Delta survival increased equilibrium abundance from the baseline of 2,097 to 2,410 spawners (+313, +14.9%), while a 10% degradation reduced it to 1,792 spawners (−305, −14.5%). The total deterministic range across the ±10% perturbation was 618 spawners. Alternatives that differ by 5% in through-Delta survival during the winter-run migration window are therefore expected to differ by approximately 154 spawners at long-term equilibrium, or roughly 7% of baseline abundance.

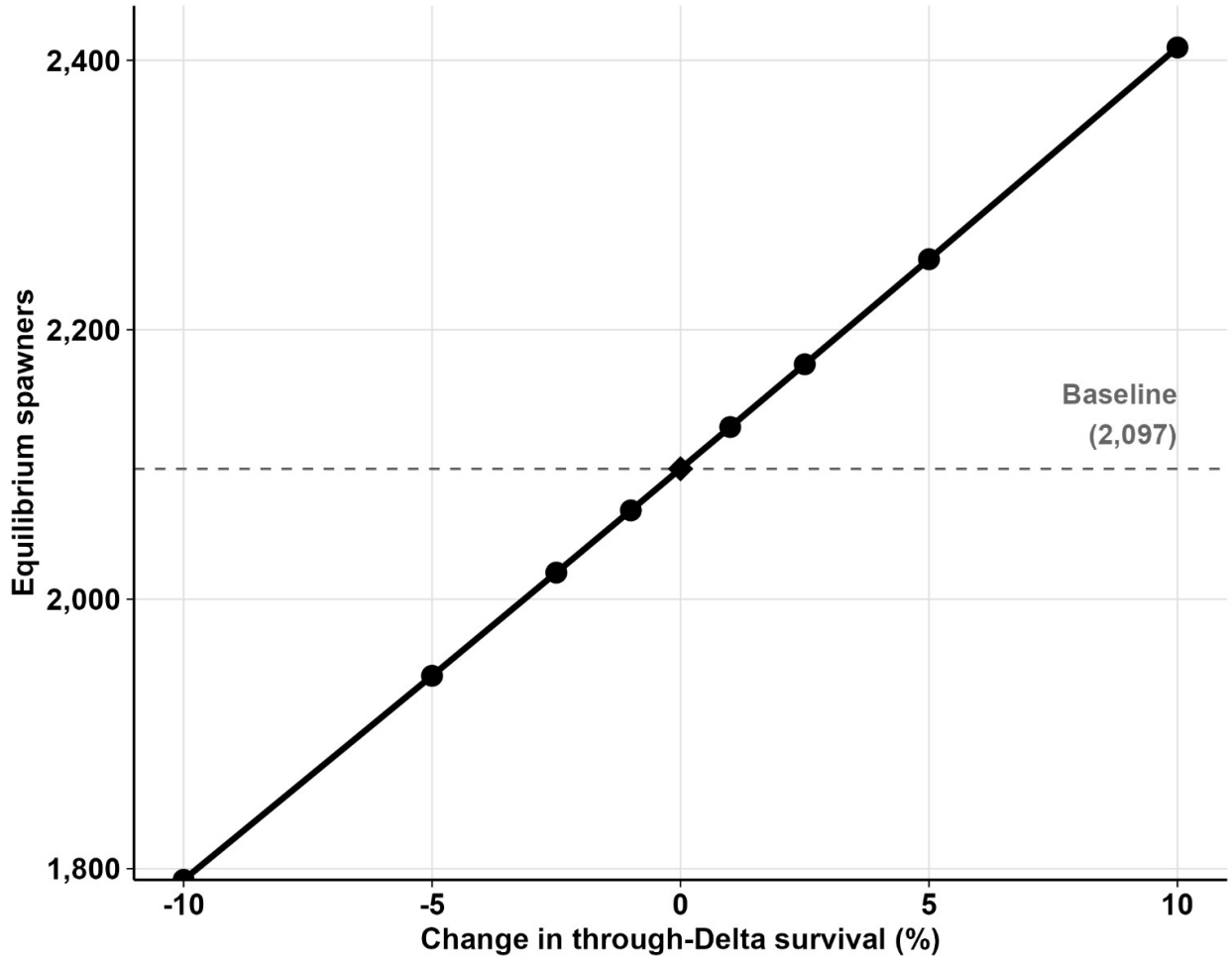


Notes: Each point represents one scenario evaluated at ±1%, ±2.5%, ±5%, and ±10% proportional perturbations from baseline ECO-PTM Delta survival. The black diamond marks the unperturbed baseline (2,904 spawners). The dashed horizontal line indicates baseline equilibrium abundance.

**Figure 9. Deterministic Dose-Response Relationship Between Proportional Changes in Through-Delta Survival and Equilibrium Spawner Abundance After 50-year Forward Projection**

## Stochastic Decomposition and Population Viability

The stochastic decomposition revealed that residual demographic variation from non-Delta processes overwhelms the operational signal at the resolution of individual brood years. Under the $M_{age2}$-only stochastic treatment, variation in the calibrated absorptive first-ocean-year parameter alone produced a 90% prediction interval of 10,021 spawners at year 50, approximately 16 times wider than the 618-spawner deterministic dose-response range (Figure 9). Under the full stochastic treatment, in which all seven empirically parameterized components varied simultaneously (Table 4), the 90% prediction interval widened to 11,034 spawners, an additional 10% of spread beyond the $M_{age2}$-only treatment (Figure 10). When each stochastic component was activated individually (Figure 11), first-ocean-year mortality produced the widest 90% prediction interval (9,901 spawners), approximately 4.5 times wider than the next largest contributor, egg-to-fry survival (2,154), followed by ocean harvest rate (1,459), hatchery juvenile production (965), maturation rates (806), adult en route survival (716), and prespawn survival (489). Individual component contributions do not sum to the full stochastic prediction interval (11,034) because the components interact nonlinearly through the density-dependent feedback loop. The aggregate comparison (Figure 11) confirms that $M_{age2}$ dominates the uncertainty budget, with the remaining six components collectively adding only 10% more variation. The dominance of $M_{age2}$ in the prediction-interval width is partly mechanical: because the calibrated value (0.971) places the parameter near the upper boundary of the survival scale, even a moderate CV (0.08) translates to a large absolute swing in cohort size when propagated through the multiplicative cohort-tracking equations. Whether this dominance persists under an alternative calibration that yields a lower $M_{age2}$ (e.g., one in which the reconstructed harvest impacts differ from those used here) is a question we revisit in the Discussion.

No scenario comparison was distinguishable from baseline under the full stochastic treatment: the proportion of iterations in which the alternative produced fewer spawners than baseline ranged from 0.48 to 0.55 across all scenarios, meaning the stochastic prediction envelopes overlap almost entirely between improved, degraded, and baseline Delta conditions (Figure 12). The full stochastic baseline produced a year-50 median of 2,410 spawners with a 90% prediction interval of [93, 11,127]. Quasi-extinction frequency at year 50 was 11.1% for the baseline scenario, with the population falling below the minimum viable threshold of 2,500 spawners in 51% of iterations. Across all scenarios, quasi-extinction frequency ranged from 8.2% to 11.1% (Figure 13), with no systematic relationship between perturbation direction or magnitude and extinction risk.

Under the paired-iteration comparison, in which demographic noise was controlled by using the same random draws for baseline and alternative runs, the Delta survival effect was consistent and unambiguous: every iteration produced fewer spawners under increased Delta mortality than under baseline conditions, across all perturbation levels. Under absolute perturbations comparable to the SRCLCM analysis, mean 10-year abundance declined from 3,360 spawners at baseline to 3,253 at 1% additional mortality (−3.2%), 2,831 at 5% (−15.7%), and 2,320 at 10% (−30.9%; 95% prediction interval: 536–5,207; Figure 14, Figure 15). The SRCLCM reported a baseline abundance of 1,879 and comparable proportional declines: −3.5% at 1%, −16.2% at 5%, and −29.8% at 10%. Both models showed approximately a 3× multiplication factor between the percentage-point mortality increase and the percent decline in abundance despite fundamentally different model architectures.

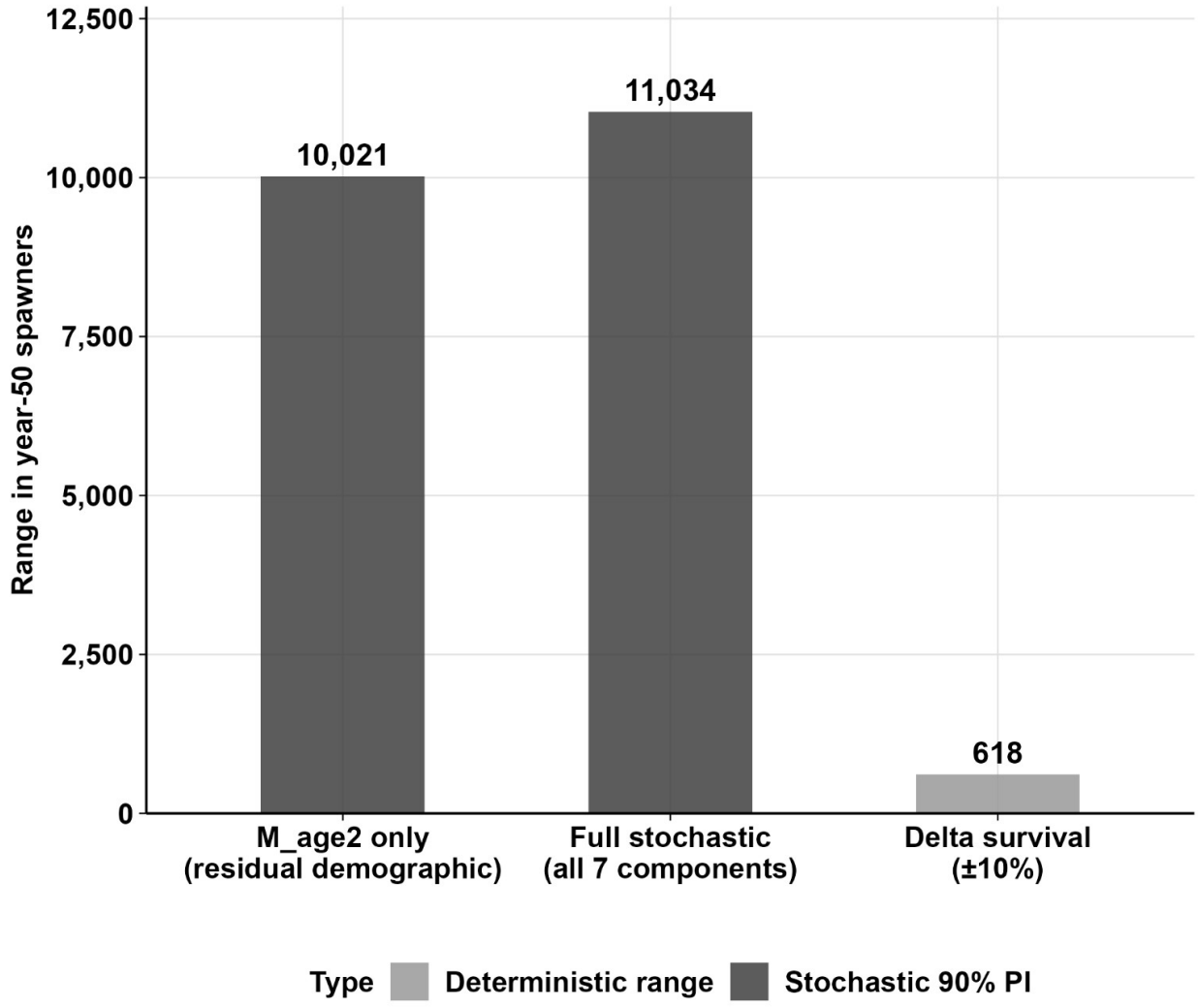


Notes: Numeric labels indicate the spawner range (5th–95th percentile width or scenario max minus min) for each source. 90% Prediction Interval from the M_age2-only Stochastic Treatment (isolating first-ocean-year mortality variation); and 90% Prediction Interval from the Full Stochastic Treatment (all empirically parameterized components; see Table 4).

**Figure 10. Magnitude of Variation in Year-50 Spawner Abundance Attributed to Three Sources: Deterministic Dose-Response Range Across all Delta Survival Perturbation Scenarios (±10%)**

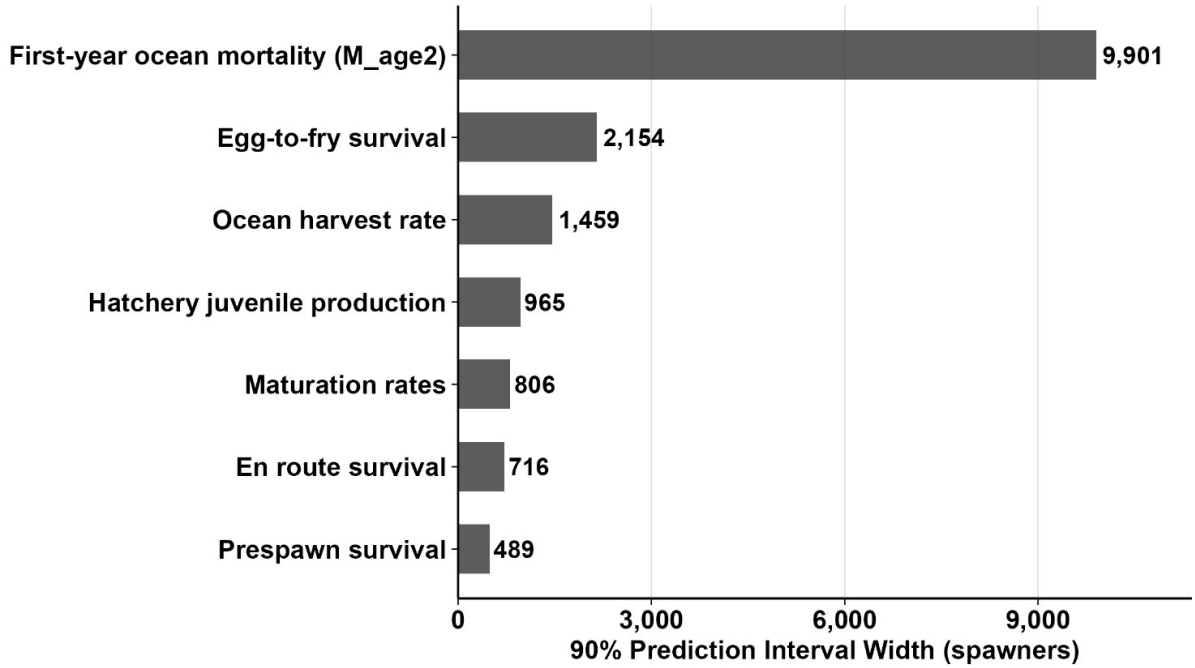


Notes: Each bar shows the interval width when only that component varies stochastically, with all others held at point estimates. Numeric labels indicate the prediction interval width in spawners.

**Figure 11. Individual Contribution of Each Stochastic Component to the 90% Prediction Interval Width in Year-50 Spawner Abundance (250 Monte Carlo iterations per component)**

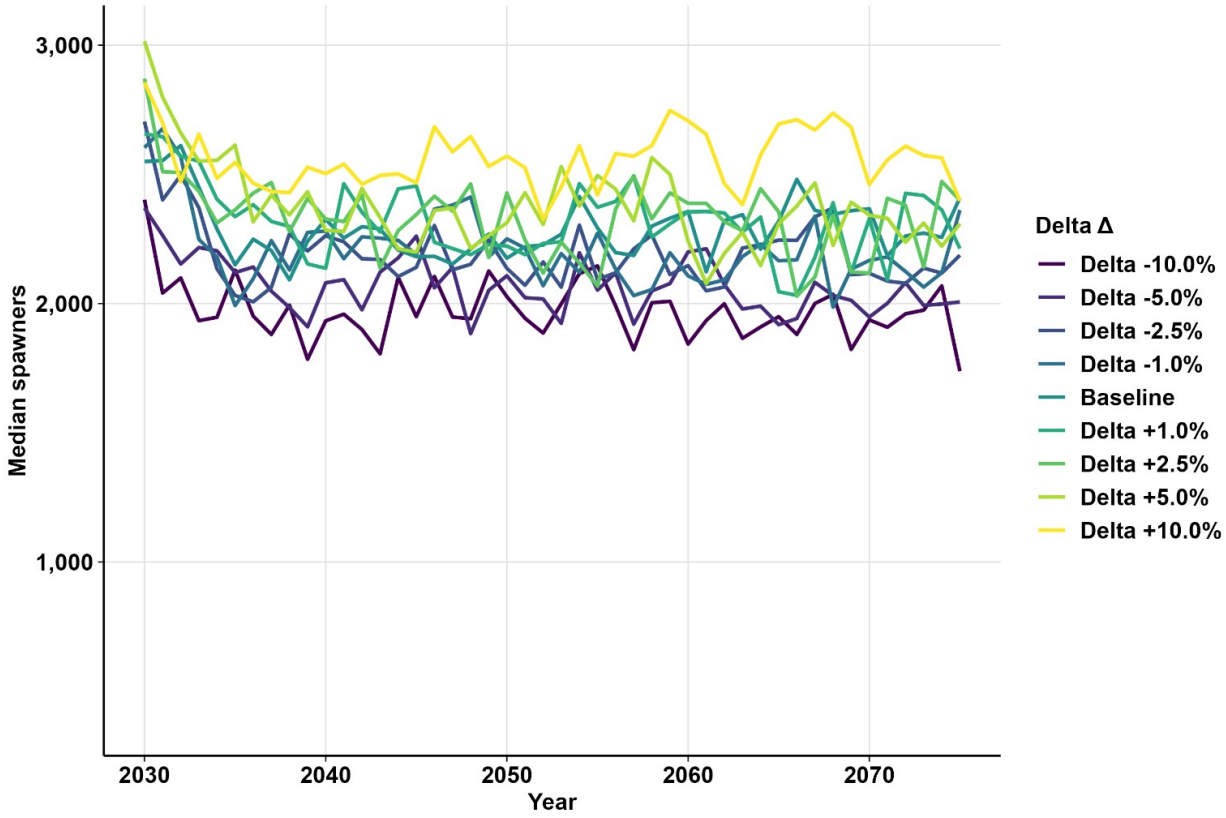


Notes: Each line represents the median trajectory across iterations for one scenario. The dotted horizontal line indicates the quasi-extinction threshold (250 spawners; Lindley et al. 2007).

**Figure 12. Median Spawner Trajectories for Delta Survival Perturbation Scenarios Under the Full Stochastic Treatment (1,000 Monte Carlo iterations per scenario)**

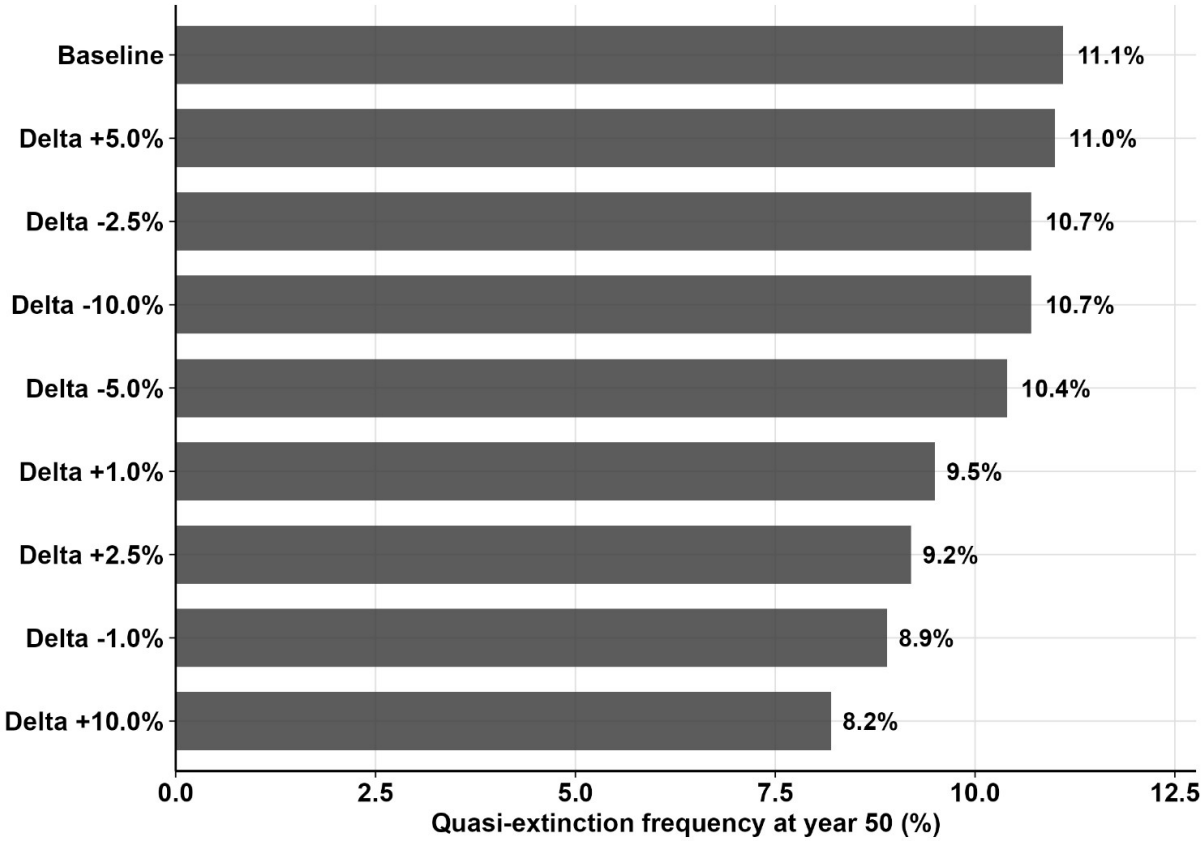


Notes: Quasi-extinction is defined as spawner abundance falling below 250 individuals in any year of the 50-year projection (Lindley et al. 2007). Numeric labels show the percentage of iterations in which quasi-extinction occurred.

**Figure 13. Quasi-extinction Frequency at Year 50 for Each Scenario Under the Full Stochastic Treatment (1,000 Monte Carlo iterations)**

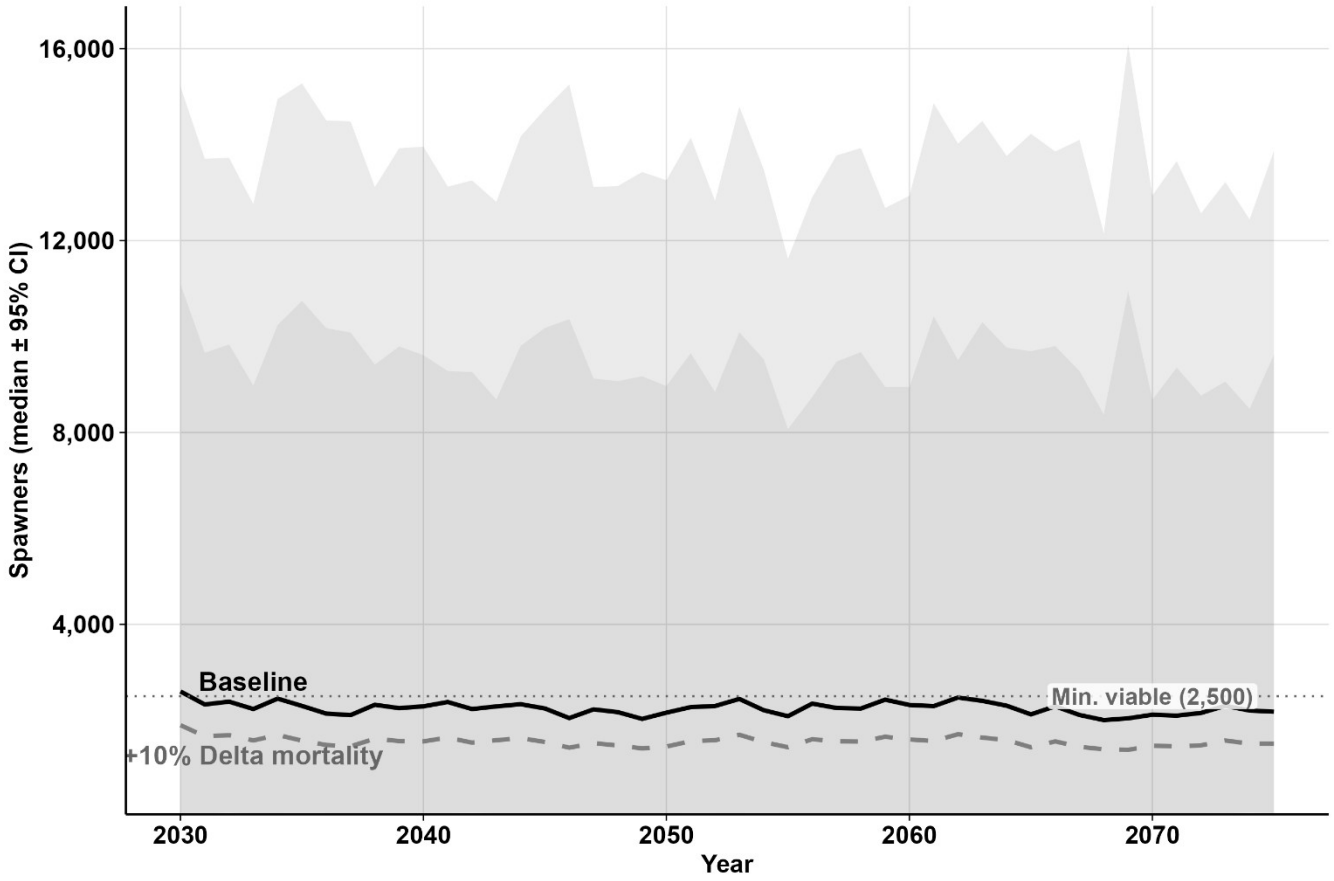


Notes: Each iteration uses the same random seed for both runs so all demographic variation cancels; the only difference is Delta survival. Solid line: baseline median. Dashed line: alternative median. Shaded ribbons: 95% prediction interval.

**Figure 14. Paired Monte Carlo Comparison of Baseline and the 10% Absolute Through-Delta Mortality Scenario (1,000 paired iterations)**

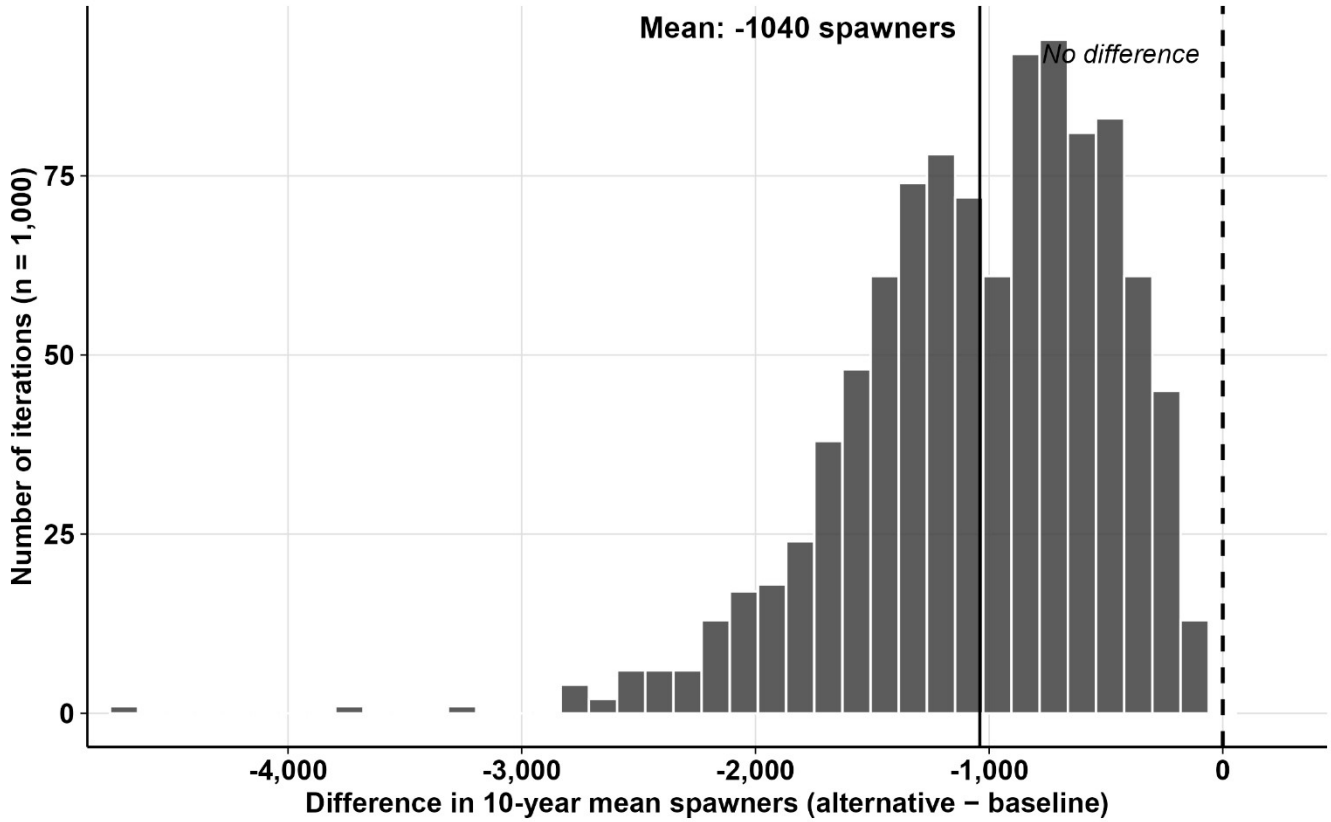


Notes: Dashed vertical line: zero (no difference). Solid vertical line: mean difference.

**Figure 15. Distribution of Paired Differences in 10-year Mean Spawner Abundance (alternative minus baseline) Across 1,000 Monte Carlo Iterations for the 10% Absolute Through-Delta Mortality Scenario**

# Sensitivity

Simulation-mode OAT sensitivity analysis revealed that first-ocean-year mortality ($M_{age2}$), adult en route survival, and through-Delta survival were tied as the most influential parameters on equilibrium spawner abundance (range = 1,231 spawners each), followed by Beverton–Holt maximum egg-to-fry survival, fecundity, rearing survival, and outmigration survival (801 each), prespawn survival (621), hatchery juvenile production (433), Beverton–Holt carrying capacity (407), ocean harvest (305), adult natural mortality (299), and maturation rates (205, 86, 72; Figure 16).

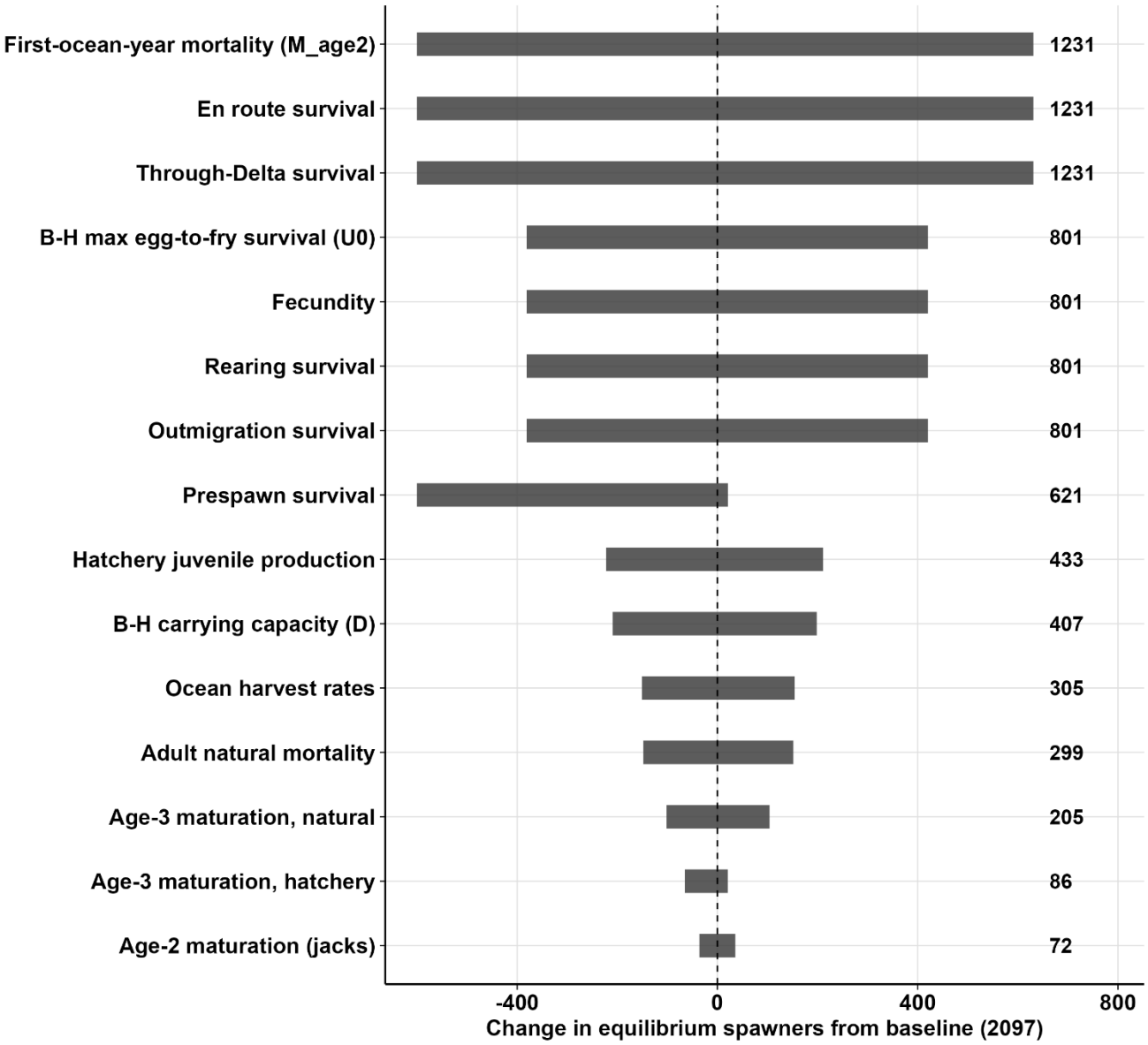


Notes: Bar length indicates the total range in equilibrium spawners between low and high perturbations; numeric labels show the range value. Parameters are ordered by decreasing sensitivity. The dashed vertical line indicates the baseline equilibrium (2,097 spawners).

**Figure 16. One-at-a-time Parameter Sensitivity Analysis (simulation mode) Showing the Change in Deterministic Equilibrium Spawner Abundance when Each of 15 Parameters is Perturbed ±20% from Baseline**

# 4. Discussion

The model was used with three complementary approaches to evaluate the population-level consequences of through-Delta survival changes; results from each are discussed in turn. The deterministic dose-response (Section 3.2) characterizes the central tendency of the translational relationship; the stochastic decomposition (Section 3.3) characterizes the demographic variation against which any operational signal must be evaluated; and the paired-iteration comparison (Section 3.3) controls demographic noise to isolate the systematic effect of Delta survival changes. Using a synthetic dose-response framework to evaluate proportional perturbations to through-Delta survival, we found that Delta survival changes produce a consistent, monotonic effect on equilibrium spawner abundance (approximately 31 spawners per 1%), but this signal is small relative to residual demographic variation from non-Delta processes. Density-dependent compensation at the egg-to-fry stage both buffers and constrains population response. It protects the population from moderate operational degradation by increasing per-capita fry production at lower spawner densities but also limits the population-level benefit of increased juvenile survival through Delta operations or reduced ocean harvest, because additional spawners face diminishing per-capita reproductive success.

Stochastic decomposition revealed that the uncertainty budget is dominated by a single source. Under the $M_{age2}$-only treatment, the calibrated absorptive parameter produced a 90% prediction interval of 10,021 spawners at year 50, approximately 16 times wider than the 618-spawner dose-response range. Adding the remaining six stochastic components widened the interval by 10% to 11,034 spawners. The true contribution of ocean conditions is unknown and likely smaller than the full $M_{age2}$ envelope, which absorbs all unmodeled processes, but ocean mortality is likely a substantial component given that winter-run reside for one to three years in the California Current (Wells et al. 2016; Gosselin et al. 2021; Kilduff et al. 2014), though $M_{age2}$ also absorbs estimation bias in upstream production, nearshore mortality, and other unmodeled processes. However, operational effects are systematic and cumulative: consistent 5% improvement shifts long-term abundance by approximately 154 fish, compounding through the density-dependent feedback loop. In the Columbia River, the Independent Scientific Advisory Board (ISAB, Jager et al 2021) cautioned against interpreting the dominance of ocean-driven variation as evidence that freshwater actions are ineffective; our results support this nuance in the Central Valley.

The paired-iteration comparison provides additional support. Under absolute perturbations, the proportional abundance response (approximately 3× the mortality increase) closely matched the winter-run life cycle model (Hendrix et al. 2014), which reported comparable proportional declines under a partially paired design using shared historical hydrology. The contrast between the paired comparison, in which every iteration produced fewer spawners under increased mortality, and the unpaired comparison ($P \approx 0.50$) illustrates the distinction between statistical detectability and biological reality: the operational effect is systematic and consistent but would be undetectable in year-to-year escapement monitoring against the background of demographic noise. The same logic explains the apparent paradox in the quasi-extinction results: under the full stochastic treatment, year-50 quasi-extinction frequency varied only between 8.2% and 11.1% across the entire ±10% perturbation range and showed no systematic relationship to perturbation direction or magnitude (Figure 13). This is not evidence that Delta survival has no effect on extinction risk; it is a

consequence of the same variance-budget result reported in Section 3.3. Quasi-extinction events (defined as any year-50 trajectory crossing 250 spawners) are dominated by tail draws of $M_{age2}$ rather than by the ~31-spawner-per-1% central-tendency shift induced by Delta survival perturbations. The paired-iteration design controls this dominant noise source by reusing identical stochastic draws across baseline and alternative runs, and it recovers a systematic, monotonic Delta survival effect that the unpaired quasi-extinction metric cannot resolve.

The dose-response framework applied the same proportional perturbation regardless of water-year conditions. In practice, export operations interact with hydrology, tidal forcing, and predator fields such that the same operational change may have larger effects in dry years. This limitation will be addressed in future applications, where scenario-specific weekly ECO-PTM survival estimates can be used as the $S_{\Delta,w}$ parameter to evaluate population-level effects of alternative Delta operations. In its current form, the framework is applicable to (1) characterizing the central-tendency translational relationship between Delta survival and equilibrium spawner abundance, and (2) comparing alternatives that differ in their weekly through-Delta survival profile under the same baseline calibration. Application to specific operational alternatives via coupling with ECO-PTM would require, at minimum: scenario-specific weekly ECO-PTM survival estimates spanning the operational range of interest; reconciliation of the ECO-PTM tagged-fish size threshold (≥140 mm fork length; Perry et al. 2018) with the smaller, earlier-migrating fraction of the natural-origin winter-run population that falls below this threshold; and accounting for temperature-dependent survival processes (e.g., thermal effects on predation rates and metabolic stress) that ECO-PTM does not currently represent. We treat these as the principal limitations to address before this framework is used to evaluate specific operational alternatives.

Delta operations alone are insufficient to drive population recovery. The deterministic baseline equilibrium of 2,097 spawners falls below the minimum viable population threshold of 2,500 (Lindley et al. 2007) even without additional Delta mortality degradation. The largest perturbation evaluated (+10%) produced an equilibrium of only 2,410 spawners, underscoring that Delta operations alone cannot drive recovery. Modeling recovery will require incorporating parameters that are influenced by management levers. The sensitivity analysis revealed that through-Delta survival has the same structural leverage as first-ocean-year mortality and adult en route survival (Figure 16), but the variance decomposition is dominated by M_age2 because it is the absorptive calibration parameter and all unmodeled variation across the life cycle is forced into it by construction. Management levers that could contribute to recovery include Delta hydrodynamic management affecting through-Delta survival (Jensen et al. 2025), cold-water pool management at Shasta Reservoir affecting fecundity and egg-to-fry survival (Martin et al. 2017), and ocean harvest management, which operates under the PFMC harvest control rule with age-3 impact rates ranging from 0% during fishery closures to approximately 28% historically (O'Farrell & Satterthwaite 2015; Chen et al. 2023). The model structure supports scenario-specific evaluation of these levers individually or as a portfolio. Decomposing the mortality currently collapsed into $M_{age2}$ into covariate-driven components, particularly ocean environmental conditions (Gosselin et al. 2021; Kilduff et al. 2014), is a priority for future development.

The calibrated M_age2 = 0.971 is conditional on the rest of the model parameterization rather than a direct biological estimate of first-ocean-year mortality. Holding other parameters fixed, higher harvest impacts in the data force M_age2 lower (more ocean entrants needed to match escapement); lower impacts force it higher. To converge to a value near the Winship et al. (2014) estimate of 0.50 would require lower egg production, higher mortality, or systematically different harvest accounting. Direct biological comparison would require harmonizing all upstream parameters between analyses.

Cross-validation supports the robustness of the calibrated value to data subsetting. All five folds converged with M_age2 ranging from 0.944 to 0.966 (mean = 0.959, SD = 0.009), a 2.2-percentage-point range that indicates the calibrated parameter is not driven by any small subset of brood years.

The model's year-to-year predictive performance is poorer than a sample-mean null model. We acknowledge this directly: the model is not a year-ahead forecasting tool. Its purpose is process-based translation of vital-rate changes into equilibrium population outcomes, something a null model cannot do. Year-to-year predictive accuracy and equilibrium-level mechanistic interpretation are separate goals not jointly maximizable here. The calibrated parameters substantially reduce predictive RMSE relative to literature-only parameterization, and the equilibrium-level results (dose-response slope, variance decomposition, paired-iteration) depend on structural relationships, not on absolute predictive accuracy.

The framework presented here is one of several quantitative approaches applied to winter-run Chinook population dynamics. The CVPIA SIT-DSM is a spatially explicit life-cycle model that tracks cohorts through freshwater habitat segments and evaluates restoration actions across the Central Valley. The SIT-DSM provides comprehensive Central Valley habitat accounting and is the source of the adult en route and prespawn survival values used here, but its Delta resolution is coarse, the Delta is treated as a single segment with a fixed survival parameter, limiting its ability to evaluate the weekly operational alternatives addressed in the present work. The original NMFS Southwest Fisheries Science Center (SWFSC) winter-run life-cycle framework (Hendrix et al. 2014) integrates temperature-dependent egg mortality, flow-mediated juvenile survival, and ocean dynamics. The Oncorhynchus Bayesian Analysis (OBAN) is a Bayesian stage-structured LCM that estimates covariate effects on stage-specific vital rates throughout the life cycle, including spawning-reach temperature, fry-rearing flows, Yolo Bypass access, Delta exports, Gulf of Farallones upwelling, and ocean harvest, with explicit posterior uncertainty propagation. Smolt-to-adult return modeling (e.g., Gosselin et al. 2021) uses environmental covariates to predict cohort-specific ocean survival but does not link to Delta operations. Relative to these frameworks, the model presented here trades mechanistic resolution at the egg-to-fry stage (Hendrix's strength), Central Valley–wide habitat detail (SIT-DSM's strength), and posterior uncertainty propagation (OBAN's strength) in exchange for transparent weekly translation of through-Delta survival into population outcomes. It is best suited to questions in which Delta passage is the dominant management lever of interest and weekly resolution within the Delta is required.

Several sources of uncertainty not represented in the current model suggest that the 16× signal-to-noise ratio is a conservative lower bound. First, the stochastic components use empirically derived CVs that capture interannual variation around mean conditions but do not represent regime-scale environmental shifts. Second, all model inputs enter as point estimates without propagation of estimation uncertainty. The stochastic variation in $M_{age2}$ (CV = 0.08), egg-to-fry survival (CV = 0.65), and other components represents observed variation of annual point estimates, not measurement or estimation error around those estimates. Year-specific vital rates from SacPAS, maturation rates from Chen et al. (2023), harvest rates from coded wire tag (CWT)-based cohort reconstruction (which depend on hatchery-origin recoveries and mixed-stock run identification with unknown precision), and weekly ECO-PTM survival estimates all enter without uncertainty intervals. A fully Bayesian treatment propagating posterior uncertainty in all parameters simultaneously would likely produce substantially wider prediction intervals, further reducing the relative magnitude of the Delta operational signal.

Other key limitations include: (1) time-varying ocean environmental and management covariates that could decompose $M_{age2}$ into covariate-driven and residual components; (2) ECO-PTM survival estimates are calibrated to acoustic-tagged juvenile Chinook ≥140 mm fork length (Perry et al. 2018), but a substantial fraction of winter-run Delta entrants are smaller than this tagging threshold, particularly early-season migrants. Smaller fish likely experience higher predation mortality and lower swimming performance, and ECO-PTM does not model temperature-dependent survival processes (e.g., thermal effects on predation rates and metabolic stress) that disproportionately affect smaller juveniles in warmer water years.; and (3) better understanding of Delta rearing habitat dynamics affecting through-Delta survival.

The Beverton–Holt carrying capacity (D) used here (1,028 redds) differs from the value reported in the cited derivation (9,107; Martin et al. 2017). Because D directly controls the spawner abundance at which density-dependent compensation begins to constrain fry production, the choice of D has a direct effect on equilibrium spawners under any given Delta survival. The sensitivity analysis (Figure 16) indicates that a ±20% perturbation in D produces a 407-spawner range in equilibrium abundance, comparable in magnitude to two-thirds of the entire ±10% Delta survival dose-response range (618 spawners). The deterministic baseline equilibrium of 2,097 spawners falling below the 2,500-spawner minimum viable population threshold is therefore conditional on the D value adopted; alternative defensible values would shift the equilibrium correspondingly. An updated SacPAS Fish Model recalibration incorporating temperature-dependent fry mortality and additional brood years is currently in progress (Beer 2024) and will become the default when finalized; the framework presented here can be re-run with the updated parameters at that time.

The life-cycle modeling framework presented here establishes a transparent, reproducible translational relationship between through-Delta survival and population-level outcomes for Sacramento River winter-run Chinook Salmon. The deterministic conversion factor of approximately 31 spawners per 1% change in Delta survival provides a first-order approximation suitable for structured comparison of operational alternatives, while the stochastic decomposition quantifies the demographic variation against which any operational signal must be evaluated. Application to future operational alternatives using scenario-specific ECO-PTM survival estimates will allow direct evaluation of how specific operational alternatives affect population-level outcomes.

# 5. References

Beer, W.N. 2024. Note on egg-to-fry recalibration. Columbia Basin Research, University of Washington. https://www.cbr.washington.edu/sacramento/fm/pdf/Note_on_Egg-to-Fry_Recalibration_v2024.pdf

Botsford, L.W., and J.G. Brittnacher. 1998. Viability of Sacramento River Winter-Run Chinook Salmon. Conservation Biology 12:65–79.

California Department of Fish and Wildlife (CDFW). 2025. GrandTab: California Central Valley Chinook Escapement Database Report. California Department of Fish and Wildlife. Available at: https://nrm.dfg.ca.gov/FileHandler.ashx?DocumentID=232739&inline=1

Chen, E.K., W.H. Satterthwaite, B.J. Kormos, R.C. Johnson, C.C. Phillis, and S.M. Carlson. 2023. Age structure of natural versus hatchery-origin endangered Chinook salmon and implications for fisheries management in California.

Crozier, L.G., B.J. Burke, B.E. Chasco, D.L. Widener, and R.W. Zabel. 2021. Climate change threatens Chinook salmon throughout their life cycle. Communications Biology 4:222.

Federal Register. 1994. Endangered and Threatened Species; Status of Sacramento River Winter- run Chinook Salmon. 1994, January 4. Available at: https://www.govinfo.gov/app/collection/fr/1994/01/Tuesday%2C%20January%204%2C%20Pages%20241-498.

Friedman, W.R., B.T. Martin, B.K. Wells, P. Warzybok, C.J. Michel, E.M. Danner, and S.T. Lindley. 2019. Modeling composite effects of marine and freshwater processes on migratory species. Ecosphere 10:e02743.

Gosselin, J.L., L.G. Crozier, and B.J. Burke. 2021. Shifting signals: Correlations among freshwater, marine and climatic indices often investigated in Pacific salmon studies. Ecological Indicators 121:107167.

Grimaldo, L.F., T. Sommer, N. Van Ark, G. Jones, E. Holland, P.B. Moyle, B. Herbold, and P. Smith. 2009. Factors Affecting Fish Entrainment into Massive Water Diversions in a Tidal Freshwater Estuary: Can Fish Losses be Managed? North American Journal of Fisheries Management 29:1253–1270.

Hendrix, N., A. Criss, E. Danner, C. M. Greene, H. Imaki, A. Pike, and S. T. Lindley. 2014. Life cycle modeling framework for Sacramento River winter-run Chinook salmon. https://repository.library.noaa.gov/view/noaa/4738.

Jager, H., Q.N. Monsen, S. Bai, Z., and E. Howe. 2021. Peer Review of the Fish and Aquatic Effects Analysis for the Long-Term Operations of the Central Valley Project and State Water Project.

Jensen A., B. Mahardja, J. Huang, S. Saadat, and J. Israel. 2025. Synthesizing Relationships Between Winter-Run Chinook Salmon Out-Migration Survival and Water Operations in the Sacramento–San Joaquin Delta. San Francisco Estuary and Watershed Science 23.

Kilduff, D.P., L.W. Botsford, and S.L.H. Teo. 2014. Spatial and temporal covariability in early ocean survival of Chinook salmon (Oncorhynchus tshawytscha) along the west coast of North America. ICES Journal of Marine Science 71:1671–1682.

Lindley, S., R. Schick, E. Mora, P. Adams, J. Anderson, S. Greene, C. Hanson, B. May, D. McEwan, B. MacFarlane, C. Swanson, and J. Williams. 2007. Framework for Assessing Viability of Threatened and Endangered Chinook Salmon and Steelhead in the Sacramento-San Joaquin Basin. San Francisco Estuary and Watershed Science 5.

Martin, B.T., A. Pike, S.N. John, N. Hamda, J. Roberts, S.T. Lindley, and E.M. Danner. 2017. Phenomenological vs. biophysical models of thermal stress in aquatic eggs. Ecology Letters 20:50–59.

Morris, M.D. 1991. Factorial Sampling Plans for Preliminary Computational Experiments. Technometrics 33.

Moussalli, E., and R. Hilborn. 1986. Optimal Stock Size and Harvest Rate in Multistage Life History Models. Canadian Journal of Fisheries and Aquatic Sciences 43:135–141.

National Marine Fisheries Service (NMFS). 2014. Recovery Plan for the Evolutionarily Significant Units of Sacramento River Winter-run Chinook Salmon and Central Valley Spring-run Chinook Salmon and the Distinct Population Segment of California Central Valley Steelhead.

National Marine Fisheries Service (NMFS). 2019. Biological Opinion on Long-term Operation of the Central Valley Project and the State Water Project. December 21, 2019.

O'Farrell, M.R., and W.H. Satterthwaite. 2015. Inferred historical fishing mortality rates for an endangered population of Chinook salmon (*Oncorhynchus tshawytscha*). Fishery Bulletin 113:341–351.

Pacific Fishery Management Council (PFMC). 2022. Preseason Report III: Council Adopted Management Measures and Environmental Assessment Part 3 for 2022 Ocean Salmon Fishery Regulations: BK78. Prepared for the Council and its advisory entities. Portland, Oregon.

Perry, R.W., P.L. Brandes, J.R. Burau, P.T. Sandstrom, and J.R. Skalski. 2015. Effect of Tides, River Flow, and Gate Operations on Entrainment of Juvenile Salmon into the Interior Sacramento–San Joaquin River Delta. Transactions of the American Fisheries Society 144:445–455.

Perry, R.W., A.C. Pope, G. Romine, P.L. Brandes, J.R. Burau, A.R. Blake, A.J. Ammann, and C.J. Michel. 2018. Flow-mediated effects on travel time, routing, and survival of juvenile Chinook salmon in a spatially complex, tidally forced river delta. Canadian Journal of Fisheries and Aquatic Sciences 75:1886–1901.

Perry, R.W., J.G. Romine, N.S. Adams, A.R. Blake, J.R. Burau, S.V. Johnston, and T.L. Liedtke. 2014. Using a Non-Physical Behavioral Barrier to Alter Migration Routing of Juvenile Chinook salmon in the Sacramento-San Joaquin River Delta. River Research and Applications 30:192–203.

Quinn, T.P. 2018. The Behavior and Ecology of Pacific Salmon and Trout. University of Washington Press, Seattle.

Scheuerell, M.D., R. Hilborn, M.H. Ruckelshaus, K.K. Bartz, K.M. Lagueux, A.D. Haas, and K. Rawson. 2006. The Shiraz model: a tool for incorporating anthropogenic effects and fish–habitat relationships in conservation planning. Canadian Journal of Fisheries and Aquatic Sciences 63:1596–1607.

U.S. Fish and Wildlife Service (USFWS). 2026. Interagency Ecological Program: Over four decades of juvenile fish monitoring data from the San Francisco Estuary, collected by the Delta Juvenile Fish Monitoring Program, 1976-2025. Environmental Data Initiative.

Wells, B.K., J.A. Santora, M.J. Henderson, P. Warzybok, J. Jahncke, R.W. Bradley, D.D. Huff, I.D. Schroeder, P. Nelson, J.C. Field, and D.G. Ainley. 2017. Environmental conditions and prey-switching by a seabird predator impact juvenile salmon survival. Journal of Marine Systems 174:54–63.

Winship, A.J., M.R. O'Farrell, W.H. Satterthwaite, B.K. Wells, and M.S. Mohr. 2015. Expected future performance of salmon abundance forecast models with varying complexity. Canadian Journal of Fisheries and Aquatic Sciences 72:557–569.

Zeug, S.C., P.S. Bergman, B.J. Cavallo, and K.S. Jones. 2012. Application of a Life Cycle Simulation Model to Evaluate Impacts of Water Management and Conservation Actions on an Endangered Population of Chinook Salmon. Environmental Modeling & Assessment 17:455–467.